JCI The Journal of Clinical Investigation

PRDM16 isoforms differentially regulate normal and leukemic hematopoiesis and inflammatory gene signature

David J. Corrigan, … , Alexandros Strikoudis, Hans-Willem Snoeck

J Clin Invest. 2018. https://doi.org/10.1172/JCI99862.

Research Article In-Press Preview **Hematology**

PRDM16 is a transcriptional co-regulator involved in translocations in acute myeloblastic leukemia (AML), myelodysplastic syndromes and T acute lymphoblastic leukemia that is highly expressed in and required for the maintenance of hematopoietic stem cells (HSCs), and can be aberrantly expressed in AML. *Prdm16* is expressed as full-length (*fPrdm16*) and short (*sPrdm16*) isoforms, the latter lacking the N-terminal PR-domain. The role of both isoforms in normal and malignant hematopoiesis is unclear. We show here that *fPrdm16* was critical for HSC maintenance, induced multiple genes involved in GTPase signaling and repressed inflammation, while *sPrdm16* supported B-cell development biased towards marginal zone B-cells and induced an inflammatory signature. In a mouse model of human MLL-AF9 leukemia *fPrdm16* extended latency, while *sPrdm16* shortened latency and induced a strong inflammatory signature, including several cytokines and chemokines that are associated with myelodysplasia and with a worse prognosis in human AML. Finally, in human NPM1-mutant and in MLL-translocated AML high expression of *PRDM16*, which negatively impacts outcome, was associated with inflammatory gene expression, thus corroborating the mouse data. Our observations demonstrate distinct roles for *Prdm16* isoforms in normal HSCs and AML, and identify *sPrdm16* as one of the drivers of prognostically adverse inflammation in leukemia.

PRDM16 isoforms differentially regulate normal and leukemic hematopoiesis and inflammatory gene signature

David J. Corrigan[1,3], Larry L. Luchsinger[1,2], Mariana Justino de Almeida[1,3], Linda J. Williams[1,2], Alexandros Strikoudis[1,2], Hans-Willem Snoeck[1,2,3,4,5]

Affiliations: [1]Columbia Center of Human Development, Columbia University Medical Center, New York, NY, USA, [2]Department of Medicine, Columbia University Medical Center, New York, NY, USA, [3]Department of Microbiology and Immunology, Columbia University Medical Center, New York, NY, USA. [4]Columbia Center for Translational Immunology, Columbia University Medical Center, New York, NY, USA

[5]Corresponding author: Black Building, Rm 801E, 650 W.168th St, New York, NY 10032, hs2680@columbia.edu; 212-342-0182

PRDM16 is a transcriptional co-regulator involved in translocations in acute myeloblastic leukemia (AML), myelodysplastic syndromes and T acute lymphoblastic leukemia that is highly expressed in and required for the maintenance of hematopoietic stem cells (HSCs), and can be aberrantly expressed in AML. *Prdm16* is expressed as full-length (*fPrdm16*) and short (*sPrdm16*) isoforms, the latter lacking the N-terminal PR-domain. The role of both isoforms in normal and malignant hematopoiesis is unclear. We show here that *fPrdm16* was critical for HSC maintenance, induced multiple genes involved in GTPase signaling and repressed inflammation, while *sPrdm16* supported B-cell development biased towards marginal zone B-cells and induced an inflammatory signature. In a mouse model of human MLL-AF9 leukemia *fPrdm16* extended latency, while *sPrdm16* shortened latency and induced a strong inflammatory signature, including several cytokines and chemokines that are associated with myelodysplasia and with a worse prognosis in human AML. Finally, in human NPM1-mutant and in MLL-translocated AML high expression of *PRDM16*, which negatively impacts outcome, was associated with inflammatory gene expression, thus corroborating the mouse data. Our observations demonstrate distinct roles for *Prdm16* isoforms in normal HSCs and AML, and identify *sPrdm16* as one of the drivers of prognostically adverse inflammation in leukemia.

INTRODUCTION

Many genes mutated or translocated in leukemia play a role in the function or development of hematopoietic stem cells (HSCs), mostly quiescent cells that reside in the bone marrow (BM), can self-renew and generate all cells of the hematopoietic system (1). One such gene is PRD-BF1 and RIZ homology (PR) domain-containing 16 (*PRDM16*), a highly conserved **(Figure S1)** 140 kDa zinc-finger transcriptional co-regulator that is a fusion partner in t(1:3)(p36;q21) and t(1;21)(p36;q22) translocations in human acute myeloblastic leukemia (AML) (2-4). Similar translocations were found in myelodysplasia (5, 6) and in adult T-cell lymphoblastic leukemia (7). *Prdm16* is selectively expressed in HSCs, and required for their maintenance (8, 9). *Prdm16* also plays important roles in non-hematopoietic tissues, as it is critical for brown fat (10, 11), craniofacial (12-15) and cardiac (16) development and for the maintenance of subventricular gray zone neural stem cells (9).

PRDM16 belongs to the PRDM protein family. In addition to *PRDM16*, several *PRDM* family members are involved in malignancy (17, 18), most notably *MDS1/EVI1* (*PRDM3*), which is translocated in AML, *BLIMP1* (*PRDM1*), which is often silenced in diffuse large B-cell lymphoma (19), and *PRDM2*, *PRDM5* and *PRDM10*, which are silenced in several solid tumors (17). Many members of the PRDM family, including PRDM16, are expressed as two distinct isoforms. Full-length proteins contain an N-terminal PR domain, with homology to SET domains, which catalyze protein lysine methylation. However, in all PRDM proteins, the most conserved region of the SET domain, responsible for its histone methyltransferase (HMT) activity, is absent (17). Full-length (f)-PRDM16 may have H3K4 or H3K9 methylation activity, however (20, 21). The three N-terminal exons of fPRDM16 are absent in the short isoform (sPRDM16) in both humans and mice, which therefore lacks the PR domain **(Figure S1)**. Potential transcription start sites (TSS) for *sPRDM16* have been suggested in exon 1, in co-transcription with *fPRDM16*, in exon 2, and in intron 3 (7, 22).

While deletion of *Prdm16* severely impairs HSC function (8, 9), the role of the individual isoforms in HSC regulation is unclear. We have previously shown that *sPrdm16* maintains elongated mitochondria in HSCs through induction of Mitofusin 2 *(Mfn2*). *Mfn2* is required for the maintenance of HSCs with extensive lymphoid potential. Expression of *Mfn2* in *Prdm16*$^{-/-}$ HSCs did not rescue function however (23). The role of *PRDM16* isoforms in hematological malignancies has also not been defined. It has been proposed that the long isoforms of several PRDM family members may be tumor suppressors in human malignancies (17, 18). This notion is based on the fact that many tumors show deletion or inactivation of a long isoform, while its overexpression induces apoptosis or cell cycle arrest. This has been demonstrated, among others, for *PRDM1* (19), *PRDM2* (24) and *PRDM5* (25). On the other hand, *PRDM14* appears to function as an oncogene in lymphoid malignancies (26). A recent study showed that *fPrdm16* inhibits MLL-AF9-mediated leukemogenesis in mice through induction of *Gfi1b*, which in turn represses *Hoxa* genes (21). This effect required H3K4 methyltransferase activity of the PR domain. In these studies, no biological role could be discerned for a methyltransferase-dead mutant, suggesting that the PR-deleted isoform of PRDM16 has no biological function. Taken together, these findings suggest that fPRDM16 is a suppressor of leukemia. However, in karyotypically normal leukemias, particularly those with nucleophosmin 1 (*NPM1*) mutations, both *PRDM16* isoforms are overexpressed to varying degrees (27), and high expression of *PRDM16* in AML is associated with worse overall survival (28-31), suggesting that although fPRDM16 is a tumor suppressor, sPRDM16 may promote leukemogenesis or leukemia progression. Several lines of evidence support a role for sPRDM16 in leukemia. In translocations involving *PRDM16*, the PR domain is often deleted (6, 7, 18, 22, 27), and sometimes only *sPRDM16* is expressed (27). These leukemias show dysplastic features and are associated with poor survival (31-33). Similarly, leukemic translocations involving the closely related family member, *PRDM3* (*MDS1/EVI1*), delete the PR domain (17, 18). The 5' region of *PRDM16* is also a frequent target of retroviral insertional mutagenesis leading to immortalization

(34) and leukemia (35) in mice. While these findings could be ascribed to deletion of a full-length tumor suppressor protein, overexpression of *sPrdm16*, but not of *fPrdm16*, in progenitor cells from *Trp53*$^{-/-}$ mice induced leukemic transformation (27). Consistent with these findings, forced expression of *sPrdm16* promoted leukemic transformation during HOXB4-mediated immortalization of HSCs (36). Collectively, these findings point towards a role for *sPRDM16* in leukemia.

We therefore examined the role of both *Prdm16* isoforms in normal HSCs and in a mouse model of human MLL-AF9 leukemia. We show here that *fPrdm16* is required for normal HSC function, while *sPrdm16* expression in HSCs induces inflammation and promotes the generation of a specific marginal zone-biased lymphoid progenitor population. Furthermore, we show that *sPrdm16* drives a prognostically adverse inflammatory signature in AML. In contrast, while physiological expression of *fPrdm16* in HSCs does not affect leukemogenesis, aberrantly expressed *fPrdm16* in leukemic cells has tumor-suppressive effects.

RESULTS

The hematopoietic phenotype of mice with conditional *Prdm16* deletion.

As germline-deleted *Prdm16*$^{-/-}$ mice die perinatally (8, 9), we generated *Prdm16*$^{fl/fl}$ mice and crossed these with *Vav-Cre* mice (37) (*Prdm16*$^{fl/fl}$*.Vav-Cre*) to determine the role of isolated deletion of *Prdm16* in the hematopoietic system **(Figure S2A,B)**. *Prdm16*$^{fl/fl}$*.Vav-Cre* mice were born in Mendelian ratios (not shown). Similar to fetal liver (FL) HSCs from *Prdm16*$^{-/-}$ mice, the frequency and absolute number of phenotypically defined BM HSCs ($Lin^-Sca1^+kit^+Flt3^-CD48^-CD150^+$, see **Figure S2C** for representative analysis gates) was reduced **(Figure 1A,B)**, while BM cellularity was similar (not shown). Peripheral white cell counts (**Figure S2D**), platelets and hemoglobin (not shown) were similar. Competitive repopulation studies, however, revealed a profound, multilineage long-term repopulation defect **(Figure 1C,D)** that became even more severe after serial transplantation **(Figure 1E)**. Limiting dilution competitive transplantation using purified HSCs revealed a decrease in functional HSC frequency in *Prdm16*$^{fl/fl}$*.Vav-Cre* mice compared to wt littermates (1/47 vs. 1/8, respectively, P=0.0006) **(Figure 1F)**. Deletion of *Prdm16* therefore not only decreased HSC number, but also impaired function of individual HSCs. The reconstitution defect in BM *Prdm16*$^{fl/fl}$*.Vav-Cre* HSCs, however, appeared less severe than that of FL HSCs from germline-deleted *Prdm16*$^{-/-}$ mice we reported previously (8). Competitive repopulation studies using *Prdm16*$^{fl/fl}$*.Vav-Cre* FL cells showed a more severe multilineage reconstitution defect similar to that previously reported by us (8) in *Prdm16*$^{-/-}$ FL HSCs, however **(Figure 1G,H)**. Cycling and apoptosis **(Figure S2E,F)** in adult BM HSCs, which were slightly but statistically significantly increased in *Prdm16*$^{-/-}$ FL HSCs (8), were marginally increased in *Prdm16*$^{fl/fl}$*.Vav-Cre* HSCs, but this difference did not reach statistical significance. Similar to germline *Prdm16*$^{-/-}$ FL cells, there was no difference in homing of donor cells to the BM after 24 hours in *Prdm16*$^{fl/fl}$*.Vav-Cre* and wt littermate BM cells **(Figure S2G)**. Conditional

deletion of *Prdm16* within the hematopoietic system therefore recapitulates the effect of germline deletion.

Genome-wide expression indicates regulation of GTPase signaling and mitochondrial metabolism by *Prdm16*.

We performed genome-wide expression analysis on RNA isolated and amplified from purified LSKCD150^{+}CD48^{-}FLT3^{-} HSCs (3 independent biological replicates, **Figure S3A,B**). RNAseq data in this publication are accessible through GEO Series accession number GSE112860 (https://www.ncbi.nlm.nih.gov/geo/query/acc.cgi?acc=GSE112860). 561 genes were significantly downregulated, while 411 genes were upregulated. As expected, *Prdm16* mRNA was reduced in *Prdm16$^{fl/fl}$.Vav-Cre* HSCs, with complete absence of exons 6 and 7, leading to a frameshift and a premature stop codon **(Figure S3C,D)**. Pathway analysis using PANTHER (38, 39) with a 0.1 false discovery rate (FDR) cut-off showed that *Prdm16* directly or indirectly regulates a broad set of pathways **(Figure 2A)**. Rho and Ras GTPase signal transduction pathways and genes regulating cell migration and vascular development, in which Rho GTPases are involved, were significantly downregulated. As Rho signaling plays a major role in HSC homing and mobilization (40), we assessed the frequency of phenotypically defined HSCs in the PB. No differences were observed between *Prdm16$^{fl/fl}$.Vav-Cre* mice and wt littermates however **(Figure 2B)**. On the other hand, pathways related to mitochondrial respiration were upregulated **(Figure 2A)**. 31 out of 96 electron transport chain (ETC) genes were overexpressed, significantly more than expected (4/96, P<0.0001) **(Figure 2C)**. Measurement of metabolism using a Seahorse metabolic flux analyzer **(Figure 2D)** revealed elevated basal oxygen consumption **(Figure 2E)** and respiratory ATP production **(Figure 2F)** in HSCs from *Prdm16$^{fl/fl}$.Vav-Cre* mice compared to *Prdm16$^{fl/fl}$* littermate HSCs. Mitochondrial ROS production was also increased **(Figure 2G).** This effect was cell type-specific as we did not observe enhanced respiration in *Prdm16$^{-/-}$* mouse embryonic fibroblasts **(Figure S3E)**.

We also compared FL *Prdm16*$^{fl/fl}$*.Vav-Cre* and wt littermate HSCs. Similar pathways (Rho and Ras GTPase signaling, blood vessel development and cell migration) were downregulated in *Prdm16*$^{fl/fl}$*.Vav-Cre* HSCs **(Figure S3F)**. No significant differences were observed in mitochondrial respiration however, indicating that regulation of respiration by *Prdm16* is specific to adult HSCs. A possible explanation is that FL stem and progenitor cells are overall more oxidative than their adult counterparts (41).

Generation of *fPrdm16*$^{-/-}$ mice.

To identify specific roles of each isoform, we used CRISPR-Cas9 by pronuclear injection of gRNA into fertilized C57BL/6 embryos (42). To target *sPrdm16*, a 500bp region in intron 3 corresponding to a putative TSS was deleted (7) **(Figure S4A)**. However, using subtractive quantitative PCR (qPCR) **(Figure S4B)**, we did not observe reduced expression of *sPrdm16* **(Figure S4C)**, although sequencing revealed that the putative TSS was deleted **(Figure S4D)**. *sPrdm16* expression in HSCs therefore likely does not depend on the TSS in intron 3. Mice were born in Mendelian ratios, developed normally (not shown), and did not show HSC defects **(Figure S4E,F)**. Targeting the *sPrdm16* start codon would also mutate a methionine (Met-186) in fPRDM16, thus complicating the assignment of any phenotype to disruption of individual PRDM16 isoforms. This strategy was therefore not pursued.

Targeting exon 2 **(Figure S5A)** yielded mouse strains with 47bp *(Δ47-fPrdm16*$^{-/-}$) and 13bp *(Δ13-fPrdm16*$^{-/-}$) frameshift deletions, respectively, leading to premature stop codons **(Figure S5B)**. Subtractive qPCR **(Figure S5C)** and exon mapping **(Figure S5D)** of RNAseq data in FL HSCs showed selective absence of *fPrdm16* mRNA. The small amount of *fPrdm16* mRNA detected would not translate to fPRDM16 protein given the frameshift within exon 2. Similar to *Prdm16*$^{-/-}$ mice, both *Δ47-fPrdm16*$^{-/-}$ and *Δ13-fPrdm16*$^{-/-}$ mice, which developed in Mendelian ratios **(Figure S5E)**, died perinatally.

Hematopoietic phenotype of *fPrdm16*$^{-/-}$ mice.

In E12.5-14.5 FL from both *Δ47-fPrdm16*$^{-/-}$ **(Figure 3A)** and *Δ13-fPrdm16*$^{-/-}$ mice **(Figure 3B),** the frequency and absolute number of HSCs was reduced although the frequency of Lin^{-} Sca1^{+}kit^{+} (LSK) cells was unchanged **(Figure S6A)**. Heterozygous mice displayed intermediate phenotypes**,** similar to *Prdm16*$^{+/-}$ mice. Given the similar phenotypes of *Δ47-fPrdm16*$^{-/-}$ and *Δ13-fPrdm16*$^{-/-}$ embryos, subsequent experiments were performed using *Δ47-fPrdm16*$^{-/-}$ embryos. The similar phenotypes of *Δ47-fPrdm16*$^{-/-}$ and *Δ13-fPrdm16*$^{-/-}$ embryos indicated that these were not caused by off-target effects. Furthermore, as any off-target indels would assort randomly after mating of *Δ47-fPrdm16*$^{+/-}$ heterozygotes and as wt littermates were used as controls, phenotypes described can be assigned with confidence to deletion of *fPrdm16*. This notion is further supported by the absence of a phenotype in mice where the putative *sPrdm16* TSS was targeted and where *fPrdm16* was intact, which can be considered non-targeting controls for *fPrdm16*. The fraction of cycling and apoptotic cells did not differ appreciably between *Δ47-fPrdm16*$^{-/-}$ and wt littermate FL HSCs **(Figure S6B,C)**. In competitive transplantation studies *Δ47-fPrdm16*$^{-/-}$ FL cells showed a severe repopulation defect in PB **(Figure 3C)** and BM **(Figure 3D)** compared to wt littermates. Similar to germline *Prdm16*$^{-/-}$ FL and to *Prdm16*$^{fl/fl}$*.Vav-Cre* BM cells, there was no defect in homing of donor cells to the BM after 24 hours in *fPrdm16*$^{-/-}$ BM cells **(Figure S5F)**. However, although FL HSCs typically show more pronounced lymphoid potential than adult BM HSCs, the *Δ47-fPrdm16*$^{-/-}$-derived donor cells displayed an even stronger and nearly absolute lymphoid bias **(Figure 3E)**, and within the lymphoid compartment, a bias towards B-cells **(Figure 3F)**. Such differentiation bias was not present in *Prdm16*$^{-/-}$ (8) or *Prdm16*$^{fl/fl}$*.Vav-Cre* HSCs **(Figure 1D,H)**. Collectively, these data indicate that *fPrdm16* is required for normal for HSC function, but that *sPrdm16* supports at least some lymphopoiesis.

Genome-wide expression profiling of *fPrdm16*$^{-/-}$ HSCs.

RNAseq on purified wt and *Δ47-fPrdm16*$^{-/-}$ HSCs revealed 578 upregulated and 694 downregulated genes in *Δ47-fPrdm16*$^{-/-}$ HSCs. Top up and downregulated genes and principal component analysis (PCA) are shown in **Figure S7**. Similar to *Prdm16*$^{fl/fl}$*.Vav-Cre* FL and adult BM HSCs, pathways involving small GTPase signaling including cell motility, Rho and Ras GTPase binding and GEF activity, actin organization, vasculogenesis and angiogenesis were downregulated in *Δ47-fPrdm16*$^{-/-}$ HSCs **(Figure 3G)**, suggesting that these pathways are specifically induced by *fPrdm16*, and that their downregulation may contribute to the severe defects in *Δ47-fPrdm16*$^{-/-}$ and *Prdm16*$^{fl/fl}$*.Vav-Cre* HSCs. A list of the top genes in these pathways reduced in both *Δ47-fPrdm16*$^{-/-}$ and *Prdm16*$^{fl/fl}$*.Vav-Cre* HSCs is given in **Table S1**. On the other hand, *Δ47-fPrdm16*$^{-/-}$ HSCs showed an increase in immune and inflammatory pathways. Although pathway analysis with rigorous multiple testing correction and an FDR cut-off of 0.1 did not reveal enhanced inflammation in wt compared to *Prdm16*$^{fl/fl}$*.Vav-Cre* HSCs, an inflammatory signature was overrepresented in wt-cells compared to *Prdm16*$^{fl/fl}$*.Vav-Cre* HSCs at an FDR of 0.13. These findings indicate that *sPrdm16* induces an inflammatory signature that is repressed by *fPrdm16.*

***sPrdm16* supports the generation of Lin-Sca1+kit- lymphoid progenitors.**

We further investigated the apparent lymphoid and B-cell bias in recipients of *Δ47-fPrdm16*$^{-/-}$ cells. Donor repopulation in recipients of *Δ47-fPrdm16*$^{-/-}$ cells was reduced to a similar extent in spleen, thymus and BM **(Figure 4A)**. In BM, donor-derived LSK cells, common lymphoid progenitors (CLPs), common myeloid progenitors (CMPs), granulocyte-monocyte progenitors (GMPs) and megakaryocyte-erythroid progenitors (MEPs) were similarly reduced in recipients of *Δ47-fPrdm16*$^{-/-}$ cells and of wt littermate cells **(Figure S6D)**. However, a population of Lin^{-}Kit^{-} Sca1^{+} (LSK^{-}) cells was strikingly overrepresented relative to other donor populations in the BM of recipients of *Δ47-fPrdm16*$^{-/-}$ cells, and were, among *Δ47-fPrdm16*$^{-/-}$ donor cells approximately

20-fold more frequent compared to donor LSK$^-$ cells in recipients of wt littermate FL cells **(Figure 4B,C)**.

Previous work from our group has shown that the LSK$^-$ population, which does not express c-KIT but expresses more SCA1 than LSK cells, contains a lymphoid progenitor distinct from CLPs, primarily possesses B-cell potential and displays a higher propensity to generate splenic marginal zone (MZ) B-cells compared to CLPs. Furthermore, B-cells generated from LSK$^-$ cells express more SCA1 than those derived from CLPs (43, 44). Analysis of the spleens of recipient mice revealed that the fraction of donor-derived MZ B-cells was significantly higher in recipients of *Δ47-fPrdm16*$^{-/-}$ cells than in recipients of wt littermate cells **(Figure 4D, Figure S6E)**. Furthermore, *Δ47-fPrdm16*$^{-/-}$ MZ B-cells expressed more SCA1 than wt littermate-derived MZ B-cells **(Figure 4E, Figure S6F)**. These findings are consistent with B-cell development that is predominantly derived from LSK$^-$ cells in *Δ47-fPrdm16*$^{-/-}$ FL cells. Further analysis of the stem and progenitor compartment in the FL of *Δ47-fPrdm16*$^{-/-}$ embryos showed lower CD150 MFI **(Figure 4F)** compared to wt littermates. As low CD150 expression is associated with higher lymphoid potential (45, 46), these findings are consistent with the lymphoid bias of *Δ47-fPrdm16*$^{-/-}$ HSCs. Finally, although LSK$^-$ cells are rare in FL (43, 44), FL from *Δ47-fPrdm16*$^{-/-}$ embryos contained more LSK$^-$ cells compared to wt **(Figure 4G)**. While highly expressed in HSCs as reported previously, *Prdm16* mRNA was nearly undetectable in LSK$^-$ cells **(Figure 4H).** It is therefore most likely that *sPrdm16* is required for the development of LSK$^-$ cells from HSCs, and not for their maintenance and differentiation into B-cells.

Collectively, these results indicate that fPrdm*16* promotes maintenance of HSCs and is not redundant with *sPrdm16*. Furthermore, both *Prdm16* isoforms play distinct roles in HSCs as they drive different genome-wide expression signatures and as *sPrdm16* is required for the development of LSK$^-$ lymphoid progenitors from HSCs.

Expression of *sPrdm16* in HSCs is sufficient to enhance the progression of leukemia

Next, we examined the role of *Prdm16* in AML using retroviral transduction of HSCs with the MLL-AF9 fusion gene and a hNFGR reporter as a model **(Figure S8A)** (47). Transduced purified adult BM *Prdm16$^{fl/fl}$.Vav-Cre*, FL *Prdm16$^{-/-}$*, FL *Δ47-fPrdm16$^{-/-}$* and appropriate wt littermate HSCs were expanded for 3-4 days, and 2x10^4 hNGFR$^+$ cells were transplanted into irradiated recipient mice together with 2x10^5 supporting wt BM cells **(Figure S8B,C)**. Multiple independent experiments from independent retroviral transductions were performed to avoid biological artifacts due to specific integration sites. Latency was significantly extended in recipients of immortalized *Prdm16$^{fl/fl}$.Vav-Cre* compared to *Prdm16$^{fl/fl}$* cells **(Figure 5A)**. However, we observed no differences in AML-CFU formation and proliferation *in vitro* **(Figure 5B)**. Leukemia was confirmed by accumulation of MAC1$^+$GR1$^+$NGFR$^+$ cells in PB **(Figure S8D)** and hematoxylin/eosin staining of PB (**Figure S8E)**. Similar data were obtained after transplantation of MLL-AF9-transduced FL HSCs from germline-deleted *Prdm16$^{-/-}$* mice **(Figure 5C,D)**. Consistent with the haploinsufficiency with respect to HSC function in *Prdm16$^{+/-}$* mice, leukemia latency in recipients of *Prdm16$^{+/-}$* cells was also intermediate between that of wt and *Prdm16$^{-/-}$* cells **(Figure 5C,D)**. Transduction of LIN$^-$SCA1$^-$KIT$^+$ progenitors (a population containing GMPs, CMPs, and MEPs) followed by transplantation also yielded a longer latency in *Prdm16*-deficient-cells **(Figure 5E)**. Retroviral transduction of both *sPrdm16* and *fPrdm16* **(Figure S8F)** partially restored latency to that of wt cells **(Figure S8G)**. In contrast, however, latency was similar in recipients of *Δ47-fPrdm16$^{-/-}$* and wt littermate immortalized cells **(Figure 5F)**. *sPrdm16* is therefore sufficient to shorten latency to that observed in recipients of wt-cells while physiological expression of *fPrdm16* in HSCs does not play a role in leukemogenesis.

To determine whether expression of *Prdm16* in leukemic cells or in the cell of origin was critical, we examined *Prdm16* mRNA expression. *Prdm16* mRNA was undetectable in leukemic cells

(Figure 5G). Expression of *sPrdm16* in the cell of origin was therefore likely the determinant of latency. An inheritable, epigenetic, leukemia-promoting effect of *sPrdm16* is therefore plausible.

RNAseq (3 independent experiments) revealed a broad array of differentially regulated pathways. 817 genes were significantly upregulated and 708 genes were downregulated in *Prdm16$^{fl/fl}$.Vav-Cre* MLL-AF9 cells. Most strikingly, inflammatory and GTPase pathways were downregulated in *Prdm16$^{fl/fl}$.Vav-Cre* leukemic cells **(Figure 5H)**. This finding is consistent with the previously described expression signature of *Prdm16$^{fl/fl}$.Vav-Cre* HSCs.

Distinct roles of *Prdm16* isoforms expressed in leukemic cells

Although *Prdm16* was undetectable in MLL-AF9 leukemic cells, aberrant expression of *PRDM16* is frequently observed in human AML and is associated with poor prognosis (27-31). We therefore examined the effect of forced expression of each isoform in leukemic cells. To avoid the confounding effect of endogenous expression of *Prdm16* in HSCs, which promotes leukemogenesis **(Figure 5)**, we transduced each isoform separately or together in MLL-AF9-immortalized HSCs from *Prdm16$^{fl/fl}$.Vav-Cre* mice **(Figure S8A,F)**. Similar GFP fluorescence indicated similar expression of each isoform in the respective lines **(Figure S8H)**. If the longer cDNA of *fPrdm16* would impair transcription or translation compared to *sPrdm16*, GFP fluorescence should be lower in cells transduced with *fPrdm16* as GFP is expressed off the IRES sequence. As with *Prdm16* deletion, there were no differences in AML-CFU or overall growth *in vitro* among MLL-AF9 cells expressing either isoform **(Figure 6A)**. However, *sPrdm16* shortened latency while *fPrdm16* further increased latency in recipients of *Prdm16$^{fl/fl}$.Vav-Cre* MLL-AF9 cells **(Figure 6B)**. Latency after co-expression of both isoforms was in between those extremes. These differences in latency were not caused by changes in engraftment, as 24-hour engraftment experiments showed that, in fact, *fPrdm16*-expressing cells engrafted more efficiently than *sPrdm16*-expressing cells **(Figure 6C)**. Cytological analysis showed increased fragmented nuclei in cells expressing *sPrdm16* **(Figure S8 I,J),** a finding consistent with the

dysplastic changes observed in AML with *Prdm16* translocations (5, 6, 18, 28, 32, 33), where the PR domain is deleted. *sPrdm16*-expressing cells also had fewer cycling cells than those expressing *fPrdm16* or empty vector **(Figure 6D)**. These findings suggest an oncogenic role for *sPrdm16* and a tumor suppressor role for *fPrdm16* when expressed in leukemic cells that is not directly related to cycling or engraftment potential.

Enhanced inflammation induced by *sPrdm16* in leukemic cells.

Expression profiles obtained by RNAseq from leukemic cells isolated from moribund mice in each cohort were compared to that of empty vector-transduced cells. 398 genes were significantly upregulated and 760 genes were significantly downregulated in *fPrdm16*-expressing *Prdm16*$^{fl/fl}$*.Vav-Cre* MLL-AF9 cells. A much larger set of genes was regulated by *sPrdm16*: 1608 genes were upregulated and 1924 genes were downregulated. The top 50 genes up and downregulated in each cohort, as well PCA are shown in **Figure S9A,B**. Differentially regulated pathways are shown in **Figure 6E and S9C**. *fPrdm16*, but not *sPrdm16*, upregulated respiration and oxidative phosphorylation pathways. Metabolic flux analysis showed that *fPrdm16*-expressing leukemic cells displayed higher basal oxygen consumption **(Figure 6F)** while higher spare respiratory capacity just failed to reach significance **(Figure 6G)** compared to control or *sPrdm16*-expressing cells. However, respiratory ATP production was similar in all groups **(Figure 6H)**, while *fPrdm16*-expressing cells displayed increased proton leak **(Figure 6I)** and ROS production **(Figure 6J)**. While enhanced uncoupling, as observed in brown fat, might play a role, no induction of *Ucp1* was observed however (not shown). On the other hand, *sPrdm16* strikingly induced immune and inflammatory pathways, a signature we also found associated with expression of *sPrdm16* in HSCs and in MLL-AF9 leukemia derived from wt compared to *Prdm16*$^{fl/fl}$*.Vav-Cre* HSCs. Of the 418 genes in the GO term 'inflammatory process', 151 were upregulated in at least one of these datasets. Of those, 56 (37%) were upregulated in at least 2, and 13 (9%) in all three datasets **(Table S2)**. *sPrdm16* also induced

several GO terms related to GTPase signaling **(Figure 6E)**. As similar pathways were found to depend on the presence of *fPrdm16* in normal HSCs, these data indicate that *sPrdm16* also has context-dependent effects on gene expression signatures. Finally, as a previous report suggested that *fPrdm16* but not a mutant without histone methyltransferase activity induces *Gfi1b* and in doing so represses *Hoxa* genes to prevent leukemogenesis (21), we specifically analyzed expression of *Gfi1b* and *Hoxa* cluster genes**.** We found however that *Gfi1b* expression was very low and that *fPrdm16* did not repress any *Hoxa* genes **(Table S3)**.

Association between *PRDM16* and inflammation in NPM1-mutant and MLL leukemias

To explore the relation between *PRDM16*, inflammation and leukemia progression in human AML, we used publicly available gene expression data from the Cancer Genome Atlas (48). Among the 179 AML samples, *PRDM16* expression (as calculated by Reads Per Kilobase of transcript per Million mapped reads [RPKM]) correlated negatively with overall survival **(Figure 7A)**, confirming multiple reports of *PRDM16* expression as a negative prognostic factor (28-31). To detect a specific impact of *sPRDM16* on prognosis, we calculated the RPKM values of exons 1-3 (*fPRDM16* only) and exons 4-17 (total *PRDM16*), using the difference between those to estimate *sPRDM16*. Expression of *fPRDM16* and *sPRDM16* were correlated indicating that both isoforms are expressed in most *PRDM16*-expressing leukemias and confirming previously published findings(27). *sPRDM16* expression, however, had a stronger negative prognostic value and more negative correlation coefficient with survival than *fPRDM16* **(Figure S10A-C)**. These data are consistent with the shortening of latency after forced expression of *sPrdm16*, but not *fPrdm16* in the MLL-AF9 mouse model, and support a primary negative prognostic role for *sPRDM16*. Notably, *PRDM16* expression was not correlated with expression of *EVI1/PRDM3* **(Figure S10D).**

We next divided the cohort into 4 quartiles based on *PRDM16* RPKM, and compared samples with low (Q1 and Q2, $PRDM16^{lo}$ with RPKM<0.1) and high (Q4, $PRDM16^{hi}$ with RPKM>5.0)

353 expression of *PRDM16* **(Figure 7B)**. Principal component analysis (PCA) showed no
354 discernable clustering **(Figure 7C).** However, among differentially expressed genes between
355 both groups HOX genes appeared overrepresented **(Table S4)**. 13/40 *HOX* genes were
356 upregulated in the *PRDM16*^{hi} cohort, significantly more than expected (0.53/40, P<0.001). We
357 compared expression of *PRDM16* after stratification based on *HOX* cluster expression, using
358 *HOXA9* and *HOXB3* as representative genes. Quite strikingly, in *HOX*-negative AML and in
359 cases where only one *HOX* cluster was upregulated, *PRDM16* expression was low to
360 undetectable. Of the 66 *HOX* negative samples, none had a *PRDM16* RPKM >5, and only 4/66
361 (6%) of cases had a *PRDM16* RPKM >1. In contrast, in *HOXA/B* double-positive AML and
362 *NPM1*-mutated AML, where both *HOXA* and *HOXB* genes are upregulated (49), the mean
363 *PRDM16* RPKM was >5 **(Figure 7D)**. As in the MLL-AF9 mouse model no repression of *HOX*
364 genes could be discerned, the association between *PRDM16* and *HOX* cluster gene expression
365 in human AML indicates that *PRDM16* does not, as has been suggested (21), repress *HOX*
366 genes, but rather that *HOX* genes may induce *PRDM16*.

367 We next focused on two specific AML subsets: karyotypically normal, *NPM1*-mutated AML (47
368 samples) because *PRDM16* is frequently overexpressed in these leukemias (27), and *MLL*-
369 rearranged leukemias (21 samples) as we found a role for *Prdm16* in the MLL-AF9 mouse
370 model and as *Prdm16* downregulation has been reported to be required for pathogenesis in this
371 model (21). As with the total AML cohort, *PRDM16* expression negatively correlated with overall
372 survival in NPM1-mutant AML **(Figure 7E)**. These effects appeared to be independent of *FLT3*
373 or *DNMT3A* co-mutations, as a negative correlation was noted in both *FLT3/DNMT3A* mutant
374 and WT populations, although sample size was likely too small to achieve statistical significance
375 (**Figure S10E,F)**. A similar trend was also present in the MLL cohort, but results were not
376 significant **(Figure 7F)**, again possibly owing to the smaller sample size.

We next divided both AML subsets into *PRDM16*^{hi} and *PRDM16*^{lo} groups, again using quartiles (Q1/Q2 vs. Q4). PCA clearly separated *PRDM16*^{hi} and *PRDM16*^{lo} groups both in *NPM1*-mutant **(Figure 7G)** and *MLL*-translocated leukemias **(Figure 7H)**. PANTHER pathway analysis showed that in both AML subsets *PRDM16*^{hi} leukemias were associated with an upregulated inflammatory signature compared to *PRDM16*^{lo} leukemias **(Figure 7I,J)**. That this association could not be detected in the overall AML cohort may indicate specificity to the NPM1 and MLL AML subsets, or be a result of using more homogenous leukemic cohorts.

Collectively, these findings indicate that *PRDM16* is associated with a worse prognosis overall, and, at least within the *NPM1*-mutant and *MLL*-translocated leukemias, with an inflammatory expression signature, consistent with the inflammatory signature induced by *sPrdm16* in the MLL-AF9 mouse model.

A core set of inflammatory genes induced by *sPrdm16* are associated with myelodysplastic syndromes.

MDS is characterized by ineffective hematopoiesis by a dominant clone displaying enhanced proliferation and cell death, while normal hematopoiesis is suppressed. Inflammation is a key feature of MDS (50, 51). As *sPrdm16*-expressing MLL-AF9 cells display dysplastic features and express an inflammatory signature **(Figure S8I,J),** we extracted all genes from the GO term 'inflammation' that were upregulated in *sPrdm16*-overexpressing compared to empty vector control and in wt compared to *Prdm16*$^{-/-}$ MLL-AF9 leukemic cells, and cross-referenced these with a consensus list of inflammatory genes frequently dysregulated in MDS (50). Of this MDS signature, a much higher fraction than expected through random association was also regulated by *sPrdm16* **(Figure 7K, Table 1)**. *sPrdm16* therefore induces an inflammatory signature that overlaps with that observed in MDS.

DISCUSSION

We report here that the two PRDM16 isoforms, sPRDM16 and fPRDM16, have distinct roles in the maintenance of HSCs and in AML.

Prdm16 is required for normal HSC function (8, 9) and conditional deletion within the hematopoietic system indicates that this effect is cell autonomous. We note that of the 14 genes found differentially regulated in germline *Prdm16*$^{-/-}$ HSCs by Fluidigm qPCR (8), only two (*Mmi1* and *Cdkn1c*) were also found in the RNAseq experiments in *Prdm16*$^{fl/fl}$*.Vav-Cre* and *Δ47-fPrdm16*$^{-/-}$ described here. The reasons may be technical. It is also possible however that the fact that we performed RNAseq on three independent replicates, thus decreasing statistical noise but increasing the probability of missing truly differentially expressed genes, may play a role. Regulation of pathways related to GTPase-mediated signaling, as well as pathways involved in cell motility and vasculogenesis, in which small GTPases play key roles, could be ascribed to expression of *fPrdm16*, which is required for HSC maintenance. These pathways play important roles in HSC function, cycling, homing and mobilization (40, 52-55). Many genes downregulated in both *Prdm16*$^{fl/fl}$*.Vav-Cre* and in *Δ47-fPrdm16*$^{-/-}$ HSCs are involved in vesicle trafficking (*Als2cl* (56), *Arhgef10* (57), *Rab11fip3* (58)) and/or are guanine exchange factors (*Arhgef10*, *Fgd5* (59), *Itsn1*, *Obscn*, *Rgl1*) **(Table S1)**. *fPrdm16* may regulate endosomal trafficking in HSCs, which may play thus far underappreciated roles in HSC function. Increased mitochondrial respiration as observed in adult, but not in fetal *Prdm16*$^{fl/fl}$*.Vav-Cre* HSCs is associated with enhanced cycling and HSC exhaustion (60-65). Cycling was only slightly enhanced in *Prdm16*-deficient HSCs, though just shy of statistical significance. The effect of *Prdm16* on respiration could not be assigned specifically to *fPrdm16*, as this effect was not present in FL HSCs and as in *Δ47-fPrdm16*$^{-/-}$ mice only FL HSCs could be assessed. It is possible that the absence of increased respiration in *Prdm16*$^{fl/fl}$*.Vav-Cre* FL HSCs is due to the

already more oxidative nature of wt FL stem and progenitor cells compared to their adult counterparts (41).

Although, unfortunately, we did not succeed in generating a *sPrdm16*$^{-/-}$ mouse, at least some of the effects of *sPrdm16* can be inferred from differences between the phenotypes resulting from deletion of both isoforms simultaneously and from deletion of *fPrdm16* alone. We have previously shown, using overexpression studies and chromatin immunoprecipitation, that *sPrdm16* induces *Mfn2* in HSCs (23). Our current studies indicate a broader role for *sPrdm16* in hematopoiesis. *sPrdm16* is required for the generation of a LSK^{-} lymphoid progenitor we described previously (43, 44), and most notably induces inflammatory pathways, both in HSCs and in leukemic cells. As inflammation is involved in HSC activation but is detrimental to HSC function when chronic (66), it is possible that specific deletion of *sPrdm16* would also reveal a critical role for this isoform and that normal HSC function hinges on the balance between both isoforms.

In contrast to the role of both *Prdm16* isoforms in the regulation of normal HSCs, we find only *sPrdm16* to be relevant for leukemogenesis from HSCs as physiological expression of *sPrdm16*, as in *Δ47-fPrdm16*$^{-/-}$ cells, is sufficient to restore the increased latency observed in *Prdm16*$^{fl/fl}$*.Vav-Cre* MLL-AF9 leukemia to that of wt. Because in these experiments *Prdm16* was not expressed in the leukemic cells, but only in the HSCs from which these were derived, it is plausible that this effect of *sPrdm16* is at least in part epigenetic, a notion consistent with previous observations suggesting that epigenetics within the cell of origin have a pronounced effect on prognosis of leukemia (67).

Consistent with the induction of an inflammatory signature in normal HSCs, *sPrdm16* also drives inflammation in MLL-AF9-induced leukemia in mice, both when expressed in HSCs and subsequently downregulated during leukemogenesis or after forced expression in leukemic cells. Multiple reports have indicated an association between inflammation and outcome in both

AML and MDS, as well as in myeloproliferative neoplasms (MPNs) and MDS/MPN (50, 51, 68-73). Anti-inflammatory and immune-suppressive treatments are currently explored in MDS (50, 51). It is unclear however which genes drive inflammation in hematological malignancies, to what extent pre-existing inflammation predisposes to the development of hematological malignancy, or whether the malignancy itself directly or indirectly promotes inflammation. The frequent association between pre-existing autoimmune disease and the subsequent development of MDS suggests that, at least in MDS, inflammation plays a role in disease predisposition, although a role for inflammation caused by or emanating from the abnormal clone in disease progression has been suggested as well (74). Our observations indicate that at least in a subset of AML, the expression of *sPRDM16* underlies an inflammatory process that originates in the leukemic clone.

The inflammatory signature induced by *sPrdm16* in leukemic cells overlapped with that observed in MDS (50, 51). A core set of genes regulated by *sPrdm16* and dysregulated in MDS (50) include cytokines and chemokines associated with prognosis in AML. High expression of hepatocyte growth factor (*HGF*) (71), vascular endothelial growth factor A (*VEGFA*) (70, 75) and tumor necrosis factor (*TNF*) (73), which are all increased in MLL-AF9 cells expressing *sPrdm16*, is associated with a worse prognosis. On the other hand, *sPrdm16* repressed *Ccl5* expression. Lower levels of *CCL5* are observed in MDS (50) and adversely affect prognosis in AML (72). The inflammatory signature induced by *sPRDM16* might explain why translocations involving *PRDM16* can also be associated with MDS (5, 6), while AML with *PRDM16* translocations displays dysplastic changes (31-33). Furthermore, we observed increased frequency of abnormal nuclei in MLL-AF9 cells expressing *sPrdm16*. Inflammatory cytokines and chemokines may suppress normal hematopoiesis, thus providing a competitive advantage to leukemic cells overexpressing *sPRDM16*, despite their lower proliferation and lower engraftment capacity. *CCL3*, for example, is also induced by *sPRDM16*, is associated with MDS (50), and inhibits

leukemic proliferation and megakaryocyte/erythroid progenitors (76). A recent report lends additional support to this idea (77). AML cells in endosteal zones of the BM express inflammatory mediators and remodel endothelial cells, thus suppressing normal hematopoiesis (77). Taken together, our observations are consistent with a model wherein *sPRDM16* induces inflammatory genes, and in particular secreted inflammatory cytokines, in leukemic cells and in doing so suppresses normal hematopoiesis, thus explaining its deleterious impact on outcome. This mechanism would also explain the absence of any effect of *Prdm16* on proliferation and colony formation of leukemic cells *in vitro*.

For many *PRDM* genes involved in malignancy, the long form functions as a tumor suppressor (19, 24, 25). Our observations suggest that physiologically expressed *fPRDM16* in HSCs does not suppress leukemogenesis, as leukemic cells from *fPrdm16*-deficient mice have similar latency to wt. Forced expression in leukemic cells, however, was associated with increased respiration and enhanced oxidative stress and extended latency, suggesting tumor suppressive activity that may counterbalance the leukemia-promoting effects of *sPRDM16* in leukemias expressing *PRDM16*. The *PRDM16* gene therefore encodes both an oncogene and a tumor suppressor. Given the negative prognostic impact of *PRDM16* and in particular of *sPRDM16* in human AML, the tumor promoting effect of *sPRDM16* appears to generally prevail over any tumor suppressive actions of *fPRDM16*.

A previous report indicated that *fPrdm16* is a tumor suppressor, but that *sPrdm16* did not promote leukemia. These authors showed that the PR domain of PRDM16 harbors H3K4 methyltransferase activity (21). Using the same MLL-AF9 model, they found that *fPrdm16*, but not a mutant (*mutPrdm16*) without H3K4 activity, induced *Gfi1b*, which in turn reduced expression of *Hoxa* cluster genes and completely prevented leukemogenesis. Furthermore, knockdown of *Prdm16* shortened latency. While we concur with Zhou et al. (21) that *Prdm16* is downregulated during MLL-AF9-induced immortalization of HSPCs, our data are at variance

with most of these findings. First of all, we do not find that *fPrdm16* blocks leukemogenesis and, in contrast to Zhou et al., we could also not detect any inhibitory effect of *fPrdm16* on proliferation *in vitro*. Second, we find that *sPrdm16*, which, similar to the mutant used by Zhou et al., cannot have any H3K4 methyltransferase activity, is biologically active, while Zhou et al. could not identify any role of *mutPrdm16*. Third, we could not find repression of *Hoxa* genes by either *Prdm16* isoform. We did observe an association between *PRDM16* and *HOX* expression in human AML however. As *Prdm16* did not affect *Hoxa* gene expression in the MLL-AF9 mouse model, *PRDM16* is likely downstream and not upstream of *HOX* genes in leukemia. Indeed, Yu et al. showed that *Hoxa9* and *Hoxa10* induced *Prdm16* (36), thus lending further support to the idea that *HOX* genes regulate *Prdm16*. There are several methodological differences between our work and that of Zhou et al. Zhou et al. evaluated the effect of *fPrdm16* and *mutPrdm16* through knockdown and forced expression approaches in a wt background. It is not clear whether or to what extent the knockdown of *Prdm16* selectively affected one or the other isoform. Furthermore, forced expression of one isoform may induce homeostatic mechanisms aimed at balancing the expression of the respective isoforms (17). In contrast, we used mice deleted for *Prdm16* or with a selective ablation of *fPrdm16*, and in addition performed overexpression experiments in *Prdm16*-deleted leukemic cells to distinguish the biological effects of each isoform.

The mechanisms of action of PRDM16 are unclear. The largely distinct expression signatures indicate distinct mechanisms and targets for each isoform. Furthermore, at least some of the expression signatures, such as mitochondrial respiration, are context-dependent. PRDM proteins act through multiple downstream mechanisms. Although some, including PRDM16 (20, 21), may harbor HMT activity, most act by recruiting other HMTs, histone deactylases and co-repressors through Zn-finger and proline-rich domains. To drive brown fat development,

PRDM16 binds C/EBPα. Furthermore, they can bind DNA directly as well. To what extent any of these mechanisms are employed by the long and short isoforms is unknown.

In summary, we showed here that s*Prdm16* and f*Prdm16* play distinct roles in the regulation of normal HSCs, and that s*Prdm16* is a driver of a prognostically adverse inflammatory signature in leukemia. The association between expression of *sPRDM16*, inflammation and progression of AML, and the similarities with MDS might foster the exploration of anti-inflammatory or immune suppressive interventions which, while unlikely to be curative, might improve prognosis of a subset of AML expressing *sPRDM16* and associated with inflammation.

METHODS

Mice

C57BL/6J mice (CD45.2) and competitor B6.SJL-Ptprca$^{Pep3b/BoyJ}$ (CD45.1) mice were purchased from the Jackson Laboratory (Bar Harbor, ME).

Prdm16$^{fl/fl}$ mice were generated by Ingenious Targeted Laboratory, Inc. (Stony Brook, NY). A neomycin resistance cassette flanked by *FRT* and a 3'*LoxP* site were inserted upstream of exon 6 and another *LoxP* site was inserted downstream of exon 7 in a 10.2Kb fragment from a C57NL/6 BAC clone, extending from intron 5 through exon 9. The modified BAC clone was electroporated into mouse ES cells, and Neo-resistant clones were expanded, screened for retention of the Neo cassette and second *LoxP* site, and injected into B6 blastocysts to generate chimeric mice. Removal of the Neo cassette was accomplished by crossing to *FLP* heterozygous mice, resulting in mutant, *Prdm16*$^{fl/fl}$ mice with *LoxP* sites flanking exon 6 and 7.

Isoform-specific *Prdm16* knockout mice were generated using CRISPR/Cas9. PX330-based plasmids (200ng/μL) (Addgene, Cambridge, MA), containing CRISPR/Cas9 expression cassettes and specific gRNAs **(Table S5)**, were injected into fertilized B6 blastocysts. Mice chimeric for CRISPR-initiated mutations were bred to WT C57BL/6J. Heterozygous siblings were mated to generate a homozygous mutant. All primers and gRNA constructs were purchased from Integrated DNA Technologies (IDT), Coralville, IA. *Prdm16*$^{-/-}$ mice were obtained from Lexicon Genetics (The Woodlands, TX) and *Vav-iCre* (*Vav-Cre*) mice were purchased from the Jackson Laboratory.

MLL-AF9 transduction and cell culture

pMSCV-FPRDM16-IRES-GFP/RFP and pMSCV-SPRDM16-IRES-GFP/RFP plasmids were cloned by XhoI/EcoRI-insertion of *fPRDM16* or *sPRDM16* cDNA into a backbone pMSCV-IRES-GFP/RFP plasmid (Addgene). pMSCV-MLL-AF9-IRES-hNGFR was cloned by replacement of

GFP from a pMSCV-MLL-AF9-IRES-GFP plasmid (Addgene) with hNGFR cDNA. Retroviral particles were produced by seeding PlatE cells (Cell Biolabs, San Diego, CA) at $7x10^5/cm^2$ overnight followed by transfection of each packaging and expression construct (1:1:1) using Lipofectamine 3000 (Invitrogen, Carlsbad, CA) according to manufacturer's instructions. Media were pooled after 48 hours, clarified and concentrated by ultracentrifugation (100,000xg), resuspended in RPMI media (Corning/Cellgro, Corning, NY) and stored at -80^{o}C. MLL-AF9 cells were generated by transduction of sorted HSCs ($Lin^-cKit^+Sca1^+Flt3^-$) or committed myeloid/erythroid progenitors ($Lin^-cKit^+Sca1^-CD16/32^+$) with an MSCV-MLL-AF9-hNGFR retroviral construct by spinfection at 750g, 22°C for 90 minutes. $hNGFR^+$ cells were sorted and expanded in RPMI media (Corning/Cellgro) containing 15% FBS (Atlanta Biologicals, Flowery Branch, GA), 1xGlutamax (Gibco, Gaithersburg, MD), penicillin/streptomycin (Gibco), 1xMEM Non-Essential Amino Acids (Gibco), SCF (50ng/mL), IL-6 (20ng/mL), and IL-3 (10ng/mL) (peptides from Peprotech, Rocky Hill, NJ). For colony-forming assays, 1000 cells were plated in 1ml media of the same composition containing 1.5% methylcellulose (Sigma-Aldrich, St. Louis MO) and colony number was counted after 7 days.

MLL-AF9 leukemia and Hematopoietic Stem Cell Transplantation

200 purified HSCs, $2x10^5$ unsorted BM or FL cells, or $2x10^4$ purified MLL-AF9 immortalized cells, as indicated, were injected together with $2x10^5$ competitor BM cells into lethally irradiated mice (two doses of 475 cGy using a Rad Source RS-200 X-ray irradiator [Rad Source, Brentwood, TN]) by tail vein injection. Survival in leukemia experiments was determined as the number of days post-transplant before mice became moribund.

Quantitative RT-PCR

After lysis (Trizol, Invitrogen, Carlsbad, CA), RNA was isolated according to manufacturer's instructions, using a chloroform/isopropanol extraction and 70% ethanol wash. cDNA was

prepared using Superscript III Reverse Transcriptase (Invitrogen). PCR was performed using the Viia7 Real-Time PCR System (Applied Biosystems, Foster City, CA), using either inventoried or custom Taqman probes, or using custom primers and SYBRGreen enzyme (**Table S5**). Relative mRNA content was determined by the ΔΔCT method normalized to GAPDH-VIC, or 18S-VIC housekeeping genes. To determine copy number of *Prdm16* isoforms, a *fPrdm16*-specific (exon 2/3 junction) and total *Prdm16* (*tPrdm16)* probe (exon 14/15 junction) were used. Copy number was calculated from a linear regression of serial dilutions of a *Prdm16*-containing plasmid, and *sPrdm16* copy number was calculated via subtraction. (*sPrdm16* = *tPrdm16* - *fPrdm16*).

Flow Cytometry and Cell Staining

Cells were analyzed on a BD LSRII or BD Fortessa flow cytometer (Becton Dickinson, Mountain View, CA). Cells were sorted using a BD Influx cell sorter. For BM analysis, bones were crushed, lysed with ACK lysis buffer, and filtered through a 0.22um filter prior to staining. For FL analysis, livers were isolated from E13-15 embryos, passed through a 0.22uM filter, and lysed with ACK buffer prior to staining. For PB analysis, blood obtained by submandibular bleeding was lysed twice with ACK buffer prior to staining. Staining was performed by incubating cells with an antibody cocktail in FACS buffer for 30 minutes at 4°C and washing in FACS buffer before analysis. Antibodies are listed in **Table S5**. All data were analyzed using FlowJo9.6 (TreeStar Inc., Ashland, OR). BM and PB from select moribund mice was stained with hematoxylin/eosin (Vector Laboratories, Burlingame, CA). Undiluted PB or BM diluted in 50uL/femur was smeared on slides, fixed with methanol, and stained with hematoxylin/eosin according to manufacturer's protocol.

Metabolic Flux Analysis

Respiratory oxygen consumption rate (OCR) was determined using a Seahorse XFe96, or XFp metabolic flux analyzer (Seahorse Bioscience, North Billerica, MA). MLL-AF9 cells ($1x10^6$ cells/well) or enriched HSCs ($Lin^-cKit^+Sca1^+Flt3^-$, $7.5x10^4$ cells/well), were suspended in unbuffered medium, equilibrated at 37^0C in a CO_2-free incubator, transferred to the Seahorse Bioanalyzer and assayed. The Mitochondrial Stress Test (Seahorse) was used to measure the respiratory properties of the cells.

Measurement of reactive oxygen species (ROS)

Cells were suspended in 500µL of PBS ($1x10^5$ cells/mL) at room temperature with 1µL CellROX Deep Red (Thermo Fisher, Waltham, MA) for 45 minutes, washed, resuspended in FACS buffer, and analyzed by flow cytometry in the APC channel. Cells treated with both CellROX and tert-butyl hydroperoxide (TBHP) were positive controls.

RNAseq analysis

mRNA from total RNA samples (400ng per sample) was enriched by poly-A pulldown. Libraries were prepared using TruSeq RNA prep kit (Illumina, San Diego, CA)) and sequenced using Illumina HiSeq2000 at the Columbia Genome Center. Samples were multiplexed in each lane. Base calling was performed using RTA (Illumina). BCL and bcl2fastq programs were used to convert BCL to FASTQ format, coupled with adaptor trimming. Reads were mapped to a reference genome (UCSC/mm9) using Tophat with 4 mismatches and 10 maximum multiple hits. Binary alignment (BAM) files were generated by Tophat to map reads to annotated genes, and converted to an annotated count matrix, using the Rsamtools and GenomicAlignments R packages. Data was then analyzed using DESeq to obtain differential expression analysis and principal component analysis. Pathway analysis was performed using PATHER, with pathway data from the GO gene ontology database.

Statistics

Statistical analysis was performed using PRISM software. Primary statistical tests include two-tailed Student's t-test for single comparisons of normally-distributed data, one-way ANOVA for multiple comparisons, Pearson's correlation test for comparisons of *PRDM16* RPKM vs survival, Gehan-Breslow-Wilcoxon log-rank tests to compare survival of recipient mice after MLL-AF9 transplantation. A P-value less than 0.05 was considered significant.

For RNAseq analysis, statistical P-values for individual genes were calculated from the DeSeq package in R using a binomial test accounting for size factors and intragene sample variance, and principal component analysis was also performed with this software. A False Discovery Rate (FDR) of less than 10% was used as the basis for a positive "hit." RNAseq Pathway analysis was performed using the PANTHER statistical overrepresentation test, with a Bonferroni correction for multiple testing. Chi-square tests were used to test whether the observed frequency of selected "hits" from RNAseq analysis were larger than the expected frequency.

Study Approval

Experiments and animal care were performed in accordance with the Columbia University Institutional Animal Care and Use Committee, under the approved mouse protocol AC-AAAM4750, of which all contributing authors are approved.

Author Contributions

HWS conceived the study and served as the primary author of the paper. DJC planned, performed, and analyzed the majority of the experiments, and helped to prepare the manuscript and figures. LLL developed the *Prdm16$^{fl/fl}$.Vav-Cre* mice, planned, performed, and analyzed experiments 1C-1F and contributed to experiments using the Seahorse bioanalyzer. LJW planned, performed and analyzed experiments 1G-H, and helped in the analysis of RNAseq data from these mice. MJA planned, performed, and executed experiments 1A-B. AS performed CuffDiff and exon analysis from *Prdm16$^{fl/fl}$.Vav-Cre* RNAseq and analyzed exons using the IGV viewer in figure S2C.

Acknowledgements

This work was supported by grant R01 CA167289, R01 HL135039, and R01 AG055910 (HWS), as well as the Ruth L. Kirschstein F31 CA196045 (DJC). Research reported in this publication was performed in the CCTI Flow Cytometry Core, supported in part by the Office of the Director, National Institutes of Health under awards S10RR027050 and S10OD020056. Research supported by the New York Stem Cell Foundation. AS is a New York Stem Cell Foundation – Druckenmiller Fellow. We thank Dr. Victor Lin from the Columbia Transgenic Mouse Shared Resource (TMSR) for advice and blastocyst injections of CRISPR/Cas9/gRNA. We also thank the JP Sulzberger Columbia Genome Center for performing RNAseq.

Conflicts of interest

The authors have declared that no conflicts of interest exist.

References

1. Rossi L, Lin KK, Boles NC, Yang L, King KY, Jeong M, Mayle A, and Goodell MA. Less is more: unveiling the functional core of hematopoietic stem cells through knockout mice. *Cell Stem Cell.* 2012;11(3):302-17.
2. Mochizuki N, Shimizu S, Nagasawa T, Tanaka H, Taniwaki M, Yokota J, and Morishita K. A novel gene, MEL1, mapped to 1p36.3 is highly homologous to the MDS1/EVI1 gene and is transcriptionally activated in t(1;3)(p36;q21)-positive leukemia cells. *Blood.* 2000;96(9):3209-14.
3. Sakai I, Tamura T, Narumi H, Uchida N, Yakushijin Y, Hato T, Fujita S, and Yasukawa M. Novel RUNX1-PRDM16 fusion transcripts in a patient with acute myeloid leukemia showing t(1;21)(p36;q22). *Genes, chromosomes & cancer.* 2005;44(3):265-70.
4. Stevens-Kroef MJ, Schoenmakers EF, van Kraaij M, Huys E, Vermeulen S, van der Reijden B, and van Kessel AG. Identification of truncated RUNX1 and RUNX1-PRDM16 fusion transcripts in a case of t(1;21)(p36;q22)-positive therapy-related AML. *Leukemia : official journal of the Leukemia Society of America, Leukemia Research Fund, UK.* 2006;20(6):1187-9.
5. Moir DJ, Jones PA, Pearson J, Duncan JR, Cook P, and Buckle VJ. A new translocation, t(1;3) (p36;q21), in myelodysplastic disorders. *Blood.* 1984;64(2):553-5.
6. Xiao Z, Zhang M, Liu X, Zhang Y, Yang L, and Hao Y. MEL1S, not MEL1, is overexpressed in myelodysplastic syndromes patients with t(1;3)(p36;q21). *Leukemia research.* 2006;30(3):332-4.
7. Yoshida M, Nosaka K, Yasunaga J, Nishikata I, Morishita K, and Matsuoka M. Aberrant expression of the MEL1S gene identified in association with hypomethylation in adult T-cell leukemia cells. *Blood.* 2004;103(7):2753-60.
8. Aguilo F, Avagyan S, Labar A, Sevilla A, Lee DF, Kumar P, Lemischka IR, Zhou BY, and Snoeck HW. Prdm16 is a physiologic regulator of hematopoietic stem cells. *Blood.* 2011;117(19):5057-66.
9. Chuikov S, Levi BP, Smith ML, and Morrison SJ. Prdm16 promotes stem cell maintenance in multiple tissues, partly by regulating oxidative stress. *Nature cell biology.* 2010;12(10):999-1006.
10. Seale P, Kajimura S, Yang W, Chin S, Rohas LM, Uldry M, Tavernier G, Langin D, and Spiegelman BM. Transcriptional control of brown fat determination by PRDM16. *Cell metabolism.* 2007;6(1):38-54.
11. Seale P, Bjork B, Yang W, Kajimura S, Chin S, Kuang S, Scime A, Devarakonda S, Conroe HM, Erdjument-Bromage H, et al. PRDM16 controls a brown fat/skeletal muscle switch. *Nature.* 2008;454(7207):961-7.
12. Bjork BC, Turbe-Doan A, Prysak M, Herron BJ, and Beier DR. Prdm16 is required for normal palatogenesis in mice. *Human molecular genetics.* 2010;19(5):774-89.
13. Shaffer JR, Orlova E, Lee MK, Leslie EJ, Raffensperger ZD, Heike CL, Cunningham ML, Hecht JT, Kau CH, Nidey NL, et al. Genome-Wide Association Study Reveals Multiple Loci Influencing Normal Human Facial Morphology. *PLoS genetics.* 2016;12(8):e1006149.
14. Ding HL, Clouthier DE, and Artinger KB. Redundant roles of PRDM family members in zebrafish craniofacial development. *Dev Dyn.* 2013;242(1):67-79.
15. Liu F, van der Lijn F, Schurmann C, Zhu G, Chakravarty MM, Hysi PG, Wollstein A, Lao O, de Bruijne M, Ikram MA, et al. A genome-wide association study identifies five loci influencing facial morphology in Europeans. *PLoS genetics.* 2012;8(9):e1002932.
16. Arndt AK, Schafer S, Drenckhahn JD, Sabeh MK, Plovie ER, Caliebe A, Klopocki E, Musso G, Werdich AA, Kalwa H, et al. Fine mapping of the 1p36 deletion syndrome identifies mutation of PRDM16 as a cause of cardiomyopathy. *American journal of human genetics.* 2013;93(1):67-77.
17. Mzoughi S, Tan YX, Low D, and Guccione E. The role of PRDMs in cancer: one family, two sides. *Current opinion in genetics & development.* 2016;36(83-91.

18. Morishita K. Leukemogenesis of the EVI1/MEL1 gene family. *International journal of hematology.* 2007;85(4):279-86.
19. Pasqualucci L, Compagno M, Houldsworth J, Monti S, Grunn A, Nandula SV, Aster JC, Murty VV, Shipp MA, and Dalla-Favera R. Inactivation of the PRDM1/BLIMP1 gene in diffuse large B cell lymphoma. *The Journal of experimental medicine.* 2006;203(2):311-7.
20. Pinheiro I, Margueron R, Shukeir N, Eisold M, Fritzsch C, Richter FM, Mittler G, Genoud C, Goyama S, Kurokawa M, et al. Prdm3 and Prdm16 are H3K9me1 methyltransferases required for mammalian heterochromatin integrity. *Cell.* 2012;150(5):948-60.
21. Zhou B, Wang J, Lee SY, Xiong J, Bhanu N, Guo Q, Ma P, Sun Y, Rao RC, Garcia BA, et al. PRDM16 Suppresses MLL1r Leukemia via Intrinsic Histone Methyltransferase Activity. *Molecular cell.* 2016.
22. Nishikata I, Sasaki H, Iga M, Tateno Y, Imayoshi S, Asou N, Nakamura T, and Morishita K. A novel EVI1 gene family, MEL1, lacking a PR domain (MEL1S) is expressed mainly in t(1;3)(p36;q21)-positive AML and blocks G-CSF-induced myeloid differentiation. *Blood.* 2003;102(9):3323-32.
23. Luchsinger LL, de Almeida MJ, Corrigan DJ, Mumau M, and Snoeck HW. Mitofusin 2 maintains haematopoietic stem cells with extensive lymphoid potential. *Nature.* 2016;529(7587):528-31.
24. He L, Yu JX, Liu L, Buyse IM, Wang MS, Yang QC, Nakagawara A, Brodeur GM, Shi YE, and Huang S. RIZ1, but not the alternative RIZ2 product of the same gene, is underexpressed in breast cancer, and forced RIZ1 expression causes G2-M cell cycle arrest and/or apoptosis. *Cancer research.* 1998;58(19):4238-44.
25. Deng Q, and Huang S. PRDM5 is silenced in human cancers and has growth suppressive activities. *Oncogene.* 2004;23(28):4903-10.
26. Dettman EJ, Simko SJ, Ayanga B, Carofino BL, Margolin JF, Morse HC, 3rd, and Justice MJ. Prdm14 initiates lymphoblastic leukemia after expanding a population of cells resembling common lymphoid progenitors. *Oncogene.* 2011;30(25):2859-73.
27. Shing DC, Trubia M, Marchesi F, Radaelli E, Belloni E, Tapinassi C, Scanziani E, Mecucci C, Crescenzi B, Lahortiga I, et al. Overexpression of sPRDM16 coupled with loss of p53 induces myeloid leukemias in mice. *J Clin Invest.* 2007;117(12):3696-707.
28. Yamato G, Yamaguchi H, Handa H, Shiba N, Kawamura M, Wakita S, Inokuchi K, Hara Y, Ohki K, Okubo J, et al. Clinical features and prognostic impact of PRDM16 expression in adult acute myeloid leukemia. *Genes, chromosomes & cancer.* 2017;56(11):800-9.
29. Shiba N, Ohki K, Kobayashi T, Hara Y, Yamato G, Tanoshima R, Ichikawa H, Tomizawa D, Park MJ, Shimada A, et al. High PRDM16 expression identifies a prognostic subgroup of pediatric acute myeloid leukaemia correlated to FLT3-ITD, KMT2A-PTD, and NUP98-NSD1: the results of the Japanese Paediatric Leukaemia/Lymphoma Study Group AML-05 trial. *British journal of haematology.* 2016;172(4):581-91.
30. Jo A, Mitani S, Shiba N, Hayashi Y, Hara Y, Takahashi H, Tsukimoto I, Tawa A, Horibe K, Tomizawa D, et al. High expression of EVI1 and MEL1 is a compelling poor prognostic marker of pediatric AML. *Leukemia : official journal of the Leukemia Society of America, Leukemia Research Fund, UK.* 2015;29(5):1076-83.
31. Duhoux FP, Ameye G, Montano-Almendras CP, Bahloula K, Mozziconacci MJ, Laibe S, Wlodarska I, Michaux L, Talmant P, Richebourg S, et al. PRDM16 (1p36) translocations define a distinct entity of myeloid malignancies with poor prognosis but may also occur in lymphoid malignancies. *British journal of haematology.* 2012;156(1):76-88.
32. Matsuo H, Goyama S, Kamikubo Y, and Adachi S. The subtype-specific features of EVI1 and PRDM16 in acute myeloid leukemia. *Haematologica.* 2015;100(3):e116-7.
33. Eveillard M, Delaunay J, Richebourg S, Lode L, Garand R, Wuilleme S, Duhoux F, Antoine-Poirel H, Godon C, and Bene MC. The closely related rare and severe acute myeloid leukemias carrying

EVI1 or PRDM16 rearrangements share singular biological features. *Haematologica.* 2015;100(3):e114-5.

34. Du Y, Jenkins NA, and Copeland NG. Insertional mutagenesis identifies genes that promote the immortalization of primary bone marrow progenitor cells. *Blood.* 2005;106(12):3932-9.
35. Modlich U, Schambach A, Brugman MH, Wicke DC, Knoess S, Li Z, Maetzig T, Rudolph C, Schlegelberger B, and Baum C. Leukemia induction after a single retroviral vector insertion in Evi1 or Prdm16. *Leukemia : official journal of the Leukemia Society of America, Leukemia Research Fund, UK.* 2008;22(8):1519-28.
36. Yu H, Neale G, Zhang H, Lee HM, Ma Z, Zhou S, Forget BG, and Sorrentino BP. Downregulation of Prdm16 mRNA is a specific antileukemic mechanism during HOXB4-mediated HSC expansion in vivo. *Blood.* 2014;124(11):1737-47.
37. de Boer J, Williams A, Skavdis G, Harker N, Coles M, Tolaini M, Norton T, Williams K, Roderick K, Potocnik AJ, et al. Transgenic mice with hematopoietic and lymphoid specific expression of Cre. *European journal of immunology.* 2003;33(2):314-25.
38. Mi H, Huang X, Muruganujan A, Tang H, Mills C, Kang D, and Thomas PD. PANTHER version 11: expanded annotation data from Gene Ontology and Reactome pathways, and data analysis tool enhancements. *Nucleic Acids Res.* 2017;45(D1):D183-D9.
39. Mi H, Muruganujan A, Casagrande JT, and Thomas PD. Large-scale gene function analysis with the PANTHER classification system. *Nat Protoc.* 2013;8(8):1551-66.
40. Nayak RC, Chang KH, Vaitinadin NS, and Cancelas JA. Rho GTPases control specific cytoskeleton-dependent functions of hematopoietic stem cells. *Immunological reviews.* 2013;256(1):255-68.
41. Manesia JK, Xu Z, Broekaert D, Boon R, van Vliet A, Eelen G, Vanwelden T, Stegen S, Van Gastel N, Pascual-Montano A, et al. Highly proliferative primitive fetal liver hematopoietic stem cells are fueled by oxidative metabolic pathways. *Stem cell research.* 2015;15(3):715-21.
42. Cong L, Ran FA, Cox D, Lin S, Barretto R, Habib N, Hsu PD, Wu X, Jiang W, Marraffini LA, et al. Multiplex genome engineering using CRISPR/Cas systems. *Science.* 2013;339(6121):819-23.
43. Kumar R, Fossati V, Israel M, and Snoeck HW. Lin-Sca1+kit- bone marrow cells contain early lymphoid-committed precursors that are distinct from common lymphoid progenitors. *J Immunol.* 2008;181(11):7507-13.
44. Fossati V, Kumar R, and Snoeck HW. Progenitor cell origin plays a role in fate choices of mature B cells. *J Immunol.* 2010;184(3):1251-60.
45. Beerman I, Bhattacharya D, Zandi S, Sigvardsson M, Weissman IL, Bryder D, and Rossi DJ. Functionally distinct hematopoietic stem cells modulate hematopoietic lineage potential during aging by a mechanism of clonal expansion. *Proc Natl Acad Sci U S A.* 2010;107(12):5465-70.
46. Weksberg DC, Chambers SM, Boles NC, and Goodell MA. CD150- side population cells represent a functionally distinct population of long-term hematopoietic stem cells. *Blood.* 2008;111(4):2444-51.
47. Milne TA. Mouse models of MLL leukemia: recapitulating the human disease. *Blood.* 2017;129(16):2217-23.
48. Cancer Genome Atlas Research N, Ley TJ, Miller C, Ding L, Raphael BJ, Mungall AJ, Robertson A, Hoadley K, Triche TJ, Jr., Laird PW, et al. Genomic and epigenomic landscapes of adult de novo acute myeloid leukemia. *The New England journal of medicine.* 2013;368(22):2059-74.
49. Spencer DH, Young MA, Lamprecht TL, Helton NM, Fulton R, O'Laughlin M, Fronick C, Magrini V, Demeter RT, Miller CA, et al. Epigenomic analysis of the HOX gene loci reveals mechanisms that may control canonical expression patterns in AML and normal hematopoietic cells. *Leukemia : official journal of the Leukemia Society of America, Leukemia Research Fund, UK.* 2015;29(6):1279-89.

50. Ganan-Gomez I, Wei Y, Starczynowski DT, Colla S, Yang H, Cabrero-Calvo M, Bohannan ZS, Verma A, Steidl U, and Garcia-Manero G. Deregulation of innate immune and inflammatory signaling in myelodysplastic syndromes. *Leukemia : official journal of the Leukemia Society of America, Leukemia Research Fund, UK.* 2015;29(7):1458-69.
51. Cull AH, and Rauh MJ. Success in bone marrow failure? Novel therapeutic directions based on the immune environment of myelodysplastic syndromes. *Journal of leukocyte biology.* 2017;102(2):209-19.
52. Gu Y, Filippi MD, Cancelas JA, Siefring JE, Williams EP, Jasti AC, Harris CE, Lee AW, Prabhakar R, Atkinson SJ, et al. Hematopoietic cell regulation by Rac1 and Rac2 guanosine triphosphatases. *Science.* 2003;302(5644):445-9.
53. Yang FC, Atkinson SJ, Gu Y, Borneo JB, Roberts AW, Zheng Y, Pennington J, and Williams DA. Rac and Cdc42 GTPases control hematopoietic stem cell shape, adhesion, migration, and mobilization. *Proc Natl Acad Sci U S A.* 2001;98(10):5614-8.
54. Zhou X, Florian MC, Arumugam P, Chen X, Cancelas JA, Lang R, Malik P, Geiger H, and Zheng Y. RhoA GTPase controls cytokinesis and programmed necrosis of hematopoietic progenitors. *The Journal of experimental medicine.* 2013;210(11):2371-85.
55. Florian MC, Dorr K, Niebel A, Daria D, Schrezenmeier H, Rojewski M, Filippi MD, Hasenberg A, Gunzer M, Scharffetter-Kochanek K, et al. Cdc42 activity regulates hematopoietic stem cell aging and rejuvenation. *Cell Stem Cell.* 2012;10(5):520-30.
56. Suzuki-Utsunomiya K, Hadano S, Otomo A, Kunita R, Mizumura H, Osuga H, and Ikeda JE. ALS2CL, a novel ALS2-interactor, modulates ALS2-mediated endosome dynamics. *Biochemical and biophysical research communications.* 2007;354(2):491-7.
57. Shibata S, Teshima Y, Niimi K, and Inagaki S. Involvement of ARHGEF10, GEF for RhoA, in Rab6/Rab8-mediating membrane traffic. *Small GTPases.* 2017:1-9.
58. Wang J, and Deretic D. The Arf and Rab11 effector FIP3 acts synergistically with ASAP1 to direct Rabin8 in ciliary receptor targeting. *Journal of cell science.* 2015;128(7):1375-85.
59. Citi S, Guerrera D, Spadaro D, and Shah J. Epithelial junctions and Rho family GTPases: the zonular signalosome. *Small GTPases.* 2014;5(4):1-15.
60. Chen C, Liu Y, Liu R, Ikenoue T, Guan KL, Liu Y, and Zheng P. TSC-mTOR maintains quiescence and function of hematopoietic stem cells by repressing mitochondrial biogenesis and reactive oxygen species. *The Journal of experimental medicine.* 2008;205(10):2397-408.
61. Mohrin M, Shin J, Liu Y, Brown K, Luo H, Xi Y, Haynes CM, and Chen D. Stem cell aging. A mitochondrial UPR-mediated metabolic checkpoint regulates hematopoietic stem cell aging. *Science.* 2015;347(6228):1374-7.
62. Maryanovich M, Zaltsman Y, Ruggiero A, Goldman A, Shachnai L, Zaidman SL, Porat Z, Golan K, Lapidot T, and Gross A. An MTCH2 pathway repressing mitochondria metabolism regulates haematopoietic stem cell fate. *Nature communications.* 2015;6(7901.
63. Takubo K, Nagamatsu G, Kobayashi CI, Nakamura-Ishizu A, Kobayashi H, Ikeda E, Goda N, Rahimi Y, Johnson RS, Soga T, et al. Regulation of glycolysis by Pdk functions as a metabolic checkpoint for cell cycle quiescence in hematopoietic stem cells. *Cell Stem Cell.* 2013;12(1):49-61.
64. Halvarsson C, Eliasson P, and Jonsson JI. Pyruvate dehydrogenase kinase 1 is essential for transplantable mouse bone marrow hematopoietic stem cell and progenitor function. *PLoS One.* 2017;12(2):e0171714.
65. Ho TT, Warr MR, Adelman ER, Lansinger OM, Flach J, Verovskaya EV, Figueroa ME, and Passegue E. Autophagy maintains the metabolism and function of young and old stem cells. *Nature.* 2017;543(7644):205-10.
66. King KY, and Goodell MA. Inflammatory modulation of HSCs: viewing the HSC as a foundation for the immune response. *Nature reviews Immunology.* 2011;11(10):685-92.

67. Krivtsov AV, Figueroa ME, Sinha AU, Stubbs MC, Feng Z, Valk PJ, Delwel R, Dohner K, Bullinger L, Kung AL, et al. Cell of origin determines clinically relevant subtypes of MLL-rearranged AML. *Leukemia.* 2013;27(4):852-60.
68. Hemmati S, Haque T, and Gritsman K. Inflammatory Signaling Pathways in Preleukemic and Leukemic Stem Cells. *Front Oncol.* 2017;7(265.
69. Deininger MWN, Tyner JW, and Solary E. Turning the tide in myelodysplastic/myeloproliferative neoplasms. *Nature reviews Cancer.* 2017;17(7):425-40.
70. Aguayo A, Kantarjian HM, Estey EH, Giles FJ, Verstovsek S, Manshouri T, Gidel C, O'Brien S, Keating MJ, and Albitar M. Plasma vascular endothelial growth factor levels have prognostic significance in patients with acute myeloid leukemia but not in patients with myelodysplastic syndromes. *Cancer.* 2002;95(9):1923-30.
71. Kim JG, Sohn SK, Kim DH, Baek JH, Lee NY, Suh JS, Chae SC, Lee KS, and Lee KB. Clinical implications of angiogenic factors in patients with acute or chronic leukemia: hepatocyte growth factor levels have prognostic impact, especially in patients with acute myeloid leukemia. *Leukemia & lymphoma.* 2005;46(6):885-91.
72. Kornblau SM, McCue D, Singh N, Chen W, Estrov Z, and Coombes KR. Recurrent expression signatures of cytokines and chemokines are present and are independently prognostic in acute myelogenous leukemia and myelodysplasia. *Blood.* 2010;116(20):4251-61.
73. Tsimberidou AM, Estey E, Wen S, Pierce S, Kantarjian H, Albitar M, and Kurzrock R. The prognostic significance of cytokine levels in newly diagnosed acute myeloid leukemia and high-risk myelodysplastic syndromes. *Cancer.* 2008;113(7):1605-13.
74. Patnaik MM, Timm MM, Vallapureddy R, Lasho TL, Ketterling RP, Gangat N, Shi M, Tefferi A, Solary E, Reichard KK, et al. Flow cytometry based monocyte subset analysis accurately distinguishes chronic myelomonocytic leukemia from myeloproliferative neoplasms with associated monocytosis. *Blood Cancer J.* 2017;7(7):e584;.
75. Aguayo A, Estey E, Kantarjian H, Mansouri T, Gidel C, Keating M, Giles F, Estrov Z, Barlogie B, and Albitar M. Cellular vascular endothelial growth factor is a predictor of outcome in patients with acute myeloid leukemia. *Blood.* 1999;94(11):3717-21.
76. Wang Y, Gao A, Zhao H, Lu P, Cheng H, Dong F, Gong Y, Ma S, Zheng Y, Zhang H, et al. Leukemia cell infiltration causes defective erythropoiesis partially through MIP-1alpha/CCL3. *Leukemia : official journal of the Leukemia Society of America, Leukemia Research Fund, UK.* 2016;30(9):1897-908.
77. Duarte D, Hawkins ED, Akinduro O, Ang H, De Filippo K, Kong IY, Haltalli M, Ruivo N, Straszkowski L, Vervoort SJ, et al. Inhibition of Endosteal Vascular Niche Remodeling Rescues Hematopoietic Stem Cell Loss in AML. *Cell Stem Cell.* 2018;22(1):64-77 e6.

902

Table 1: Genes differentially expressed by *sPrdm16*-expressing leukemia and MDS

		Prdm16$^{fl/fl}$.*Vav-Cre* (KO) vs *Prdm16*$^{fl/fl}$ (WT) MLL-AF9		empty vector MLL-AF9 vs. *sPrdm16*-MLL-AF9	
	change in MDS	fold change	P-value	fold change	P-value
Ccl5	Lower	0.34	9.4E-03	0.32	3.5E-03
Csf1r	Higher	2.00	1.9E-02	3.58	8.4E-05
Tnf	Higher	3.12	5.1E-08	3.27	1.4E-05
Il1r2	Higher	2.60	4.1E-02	11.28	3.9E-06
Il15	Higher	2.29	7.9E-05	4.47	4.2E-16
Vegfa	Higher	*1.06*	*6.9E-01*	1.49	1.0E-02
Ccl3	Higher	3.33	7.2E-04	2.47	2.0E-04
Ccl4	Higher	2.69	9.0E-03	2.58	6.1E-03
Hgf	Higher	*1.18*	*4.8E-01*	3.28	3.6E-07
Tlr2	Higher	0.92	6.2E-01	2.43	1.4E-05
Tlr9	Higher	2.71	9.2E-03	1.96	3.4E-02

903
904

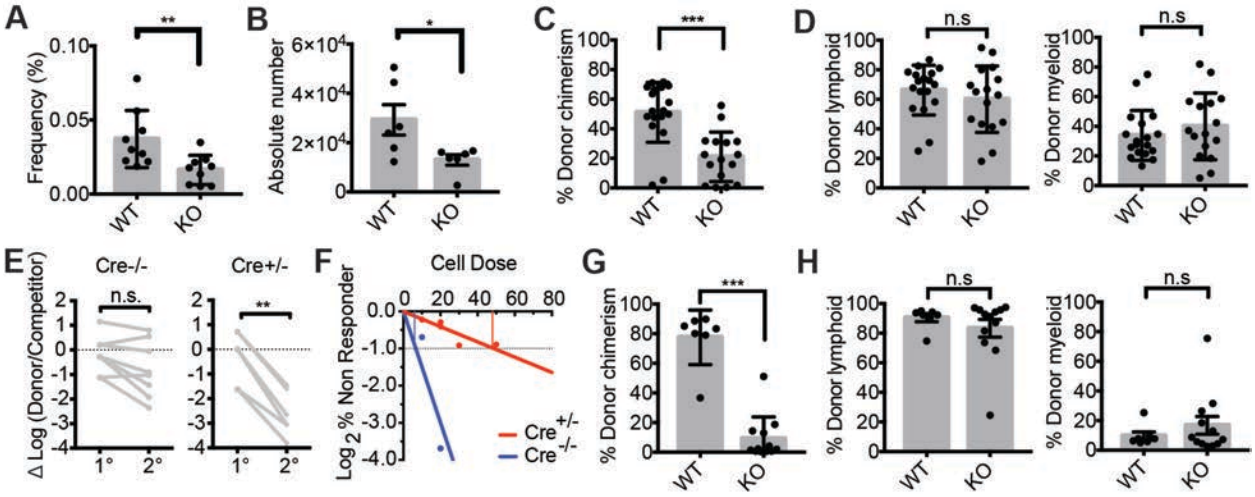

Figure 1: ***Prdm16 supports normal*** **HSC function** (**A**) Frequency (n = 9) and (**B**) absolute number (n = 6) of HSCs ($LIN^-cKIT^+SCA1^+FLT3^-CD48^-CD150^+$) in BM of adult *Vav-Cre*$^{-/-}$ *Prdm16*$^{fl/fl}$ (WT) and *Vav-Cre*$^{+/-}$ *Prdm16*$^{fl/fl}$ (KO) mice (**C**) Peripheral blood (PB) donor chimerism of WT or KO BM HSCs in competitive transplants with CD45.1 BM 16-weeks post-transplant. (n = 16-18 mice, 3 independent transplants). (**D**) Percent lymphoid ($CD19^+$ or $CD3^+$) and myeloid ($Gr\text{-}1^+$ or $Mac1^+$) donor cells from (C) (n = 16-18 mice). (**E**) Change in donor/competitor ratio (log_{10} scale) in primary competitive transplantation recipients and secondary recipients. (n = 8 mice, 2 independent transplants). (**F**) Limiting dilution assay of WT vs KO BM HSCs. (**G**) PB donor chimerism of WT or KO FL HSCs 16 weeks after competitive transplantation (n = 8-10 mice, 2 independent transplants) (**H**) Percentage of donor lymphoid or myeloid donor cells from (G) (n = 8-10 mice). (mean ± SEM; n.s:$P > 0.05$; *$P < 0.05$; **$P < 0.01$; ***$P < 0.001$, Student's t-test).

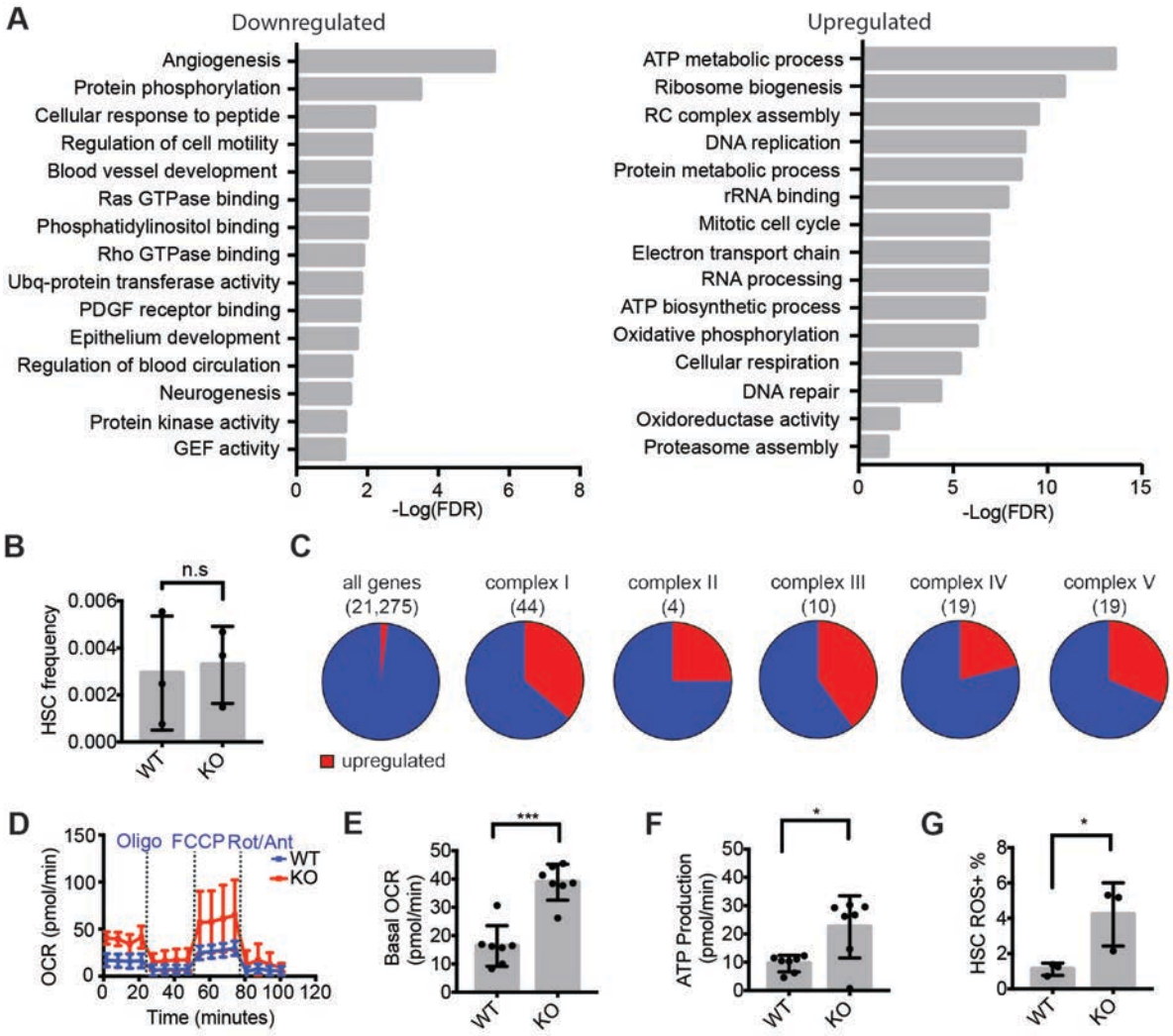

Figure 2: Increased respiration in adult *Prdm16*-deficient HSCs (**A**) GO pathways significantly up/downregulated in *Prdm16*-deficient HSCs. Values expressed as $-\text{Log}_{10}$ of the P-value, determined by PANTHER analysis. (**B**) HSC frequency in PB of *Vav-Cre*$^{-/-}$ *Prdm16*$^{fl/fl}$ (WT) and *Vav-Cre*$^{+/-}$ *Prdm16*$^{fl/fl}$ (KO) mice. (*n* = 3). (**C**) Fraction of genes upregulated (red) in *Prdm16*-deficient HSCs among all genes and the five respiratory complexes. (**D**) Extracellular metabolic flux analysis of WT and KO BM HSCs (*n* = 3 experiments in duplicate, 5 mice/experiment). (**E**) Basal oxygen consumption rate (OCR) and (**F**) Respiratory ATP production measured from (D) (*n* = 3). (**G**) Reactive oxygen species (ROS) measured by the percentage of CellROX-Deep Red positive WT or KO BM HSCs (*n* = 3). (mean ± SEM; n.s:*P* > 0.05; **P* < 0.05; ***P* < 0.01; ****P* < 0.001, Student's t-test, and Chi-square test for observed vs. expected values).

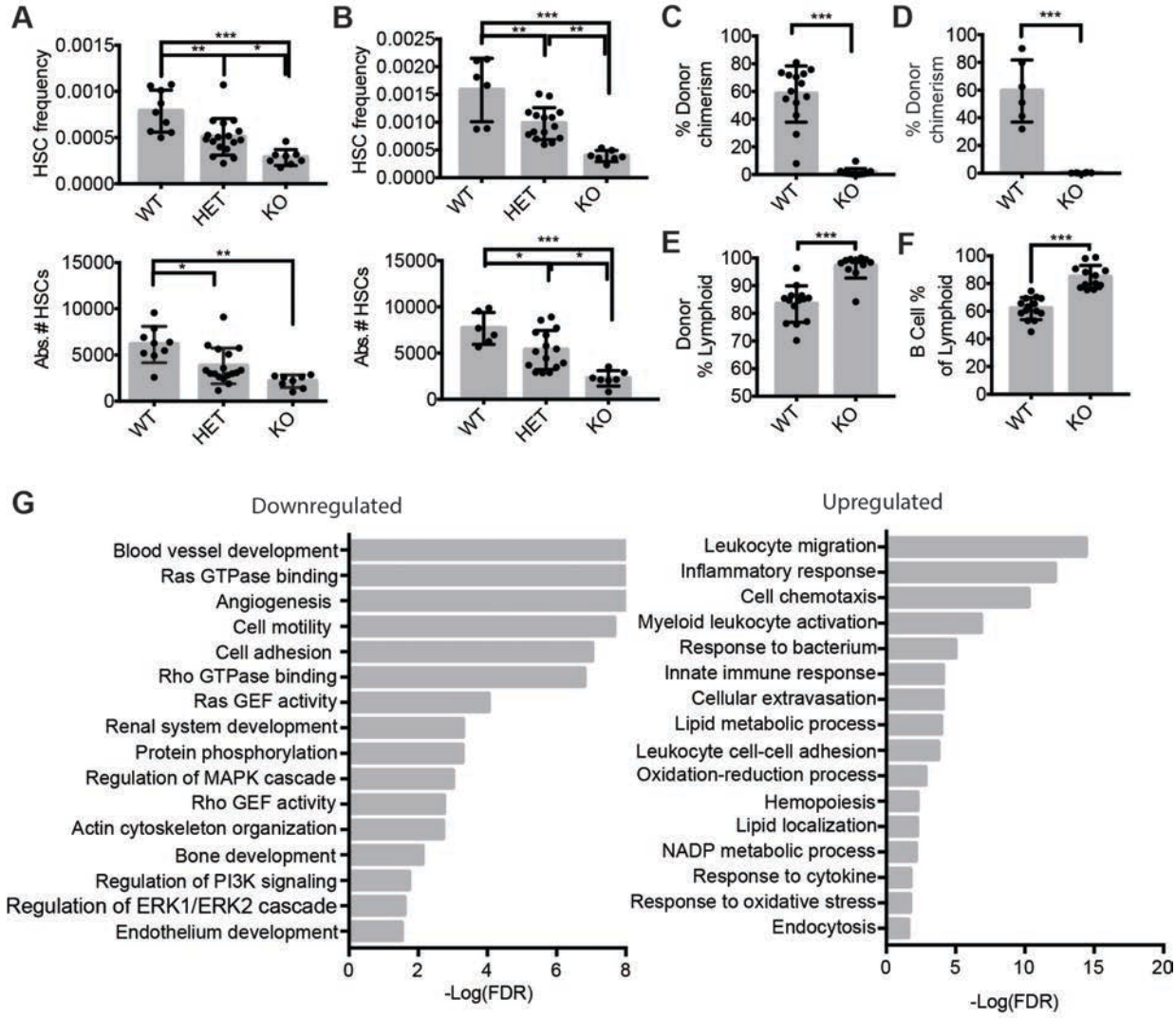

Figure 3: Hematopoietic phenotype of *fPrdm16*-deficient mice. (**A**) HSC frequency and absolute number ($LIN^-cKIT^+SCA^+MAC1^+CD48^-CD150^+$) in FL of *Δ47-fPrdm16*$^{-/-}$ (KO), *Δ47-fPrdm16*$^{+/-}$ (HET) and WT littermate mice (*n* = 34 mice). (**B**) Analysis of *Δ13-fPrdm16*$^{-/-}$ mice, performed as in (A) (*n* = 28 mice). (**C**) PB donor chimerism 16 weeks after competitive transplantation of WT or KO FL HSCs (*n* = 12-14 mice, 3 independent experiments). (**D**) BM donor chimerism in recipient mice from (C) 16 weeks after transplantation. (*n* = 6 mice). (**E**) Percent lymphoid ($CD19^+$ or $CD3^+$) donor cells in PB from (C) (*n* = 12-14). (**F**) Percent of B-cells ($CD19^+$) among lymphoid cells in (E). (**G**) GO pathways significantly up/downregulated in *Δ47-fPrdm16*$^{-/-}$ FL HSCs. Values expressed as $-Log_{10}$ of the P-value, determined by PANTHER analysis. (mean ± SEM; n.s:$P > 0.05$; *$P < 0.05$; **$P < 0.01$; ***$P < 0.001$, One-way ANOVA for multiple comparisons or Student's t-test for single comparisons).

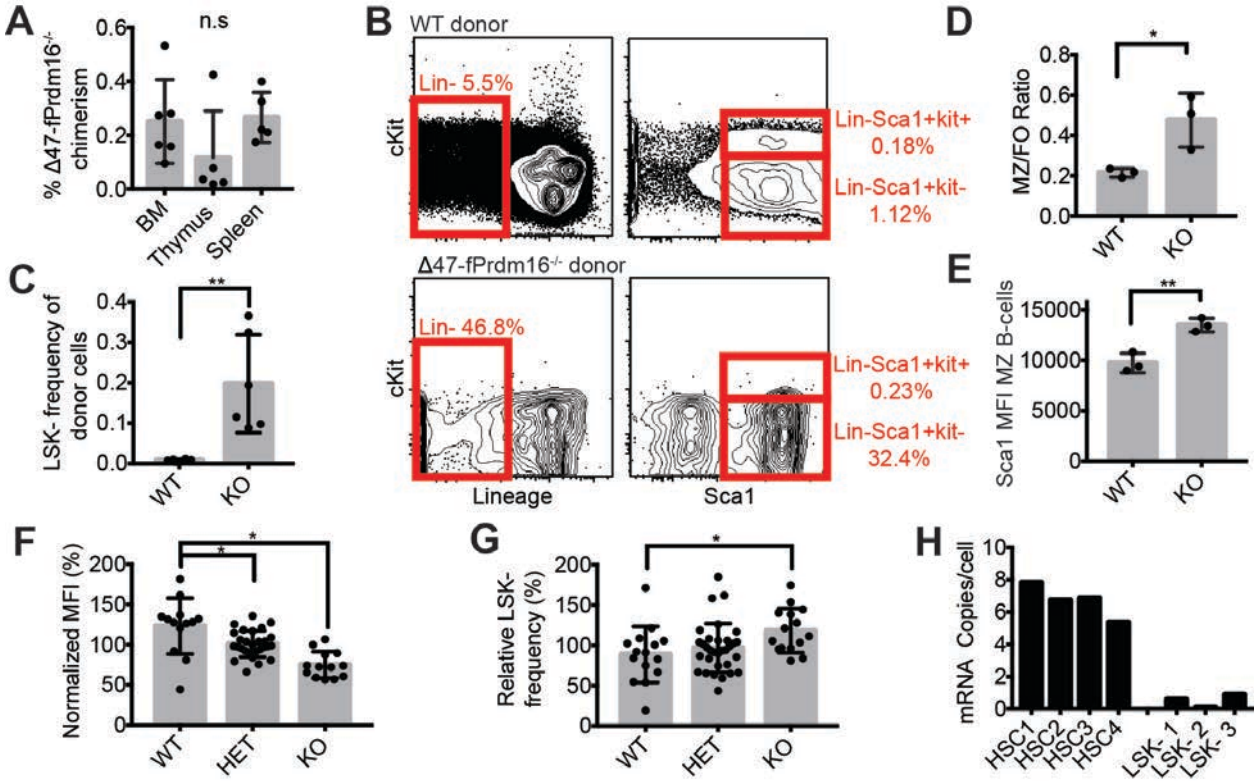

Figure 4: *sPrdm16* supports development of a LSK$^-$ B-cell progenitor (**A**) Donor chimerism in BM, thymus, and spleen 16 weeks after competitive transplantation of *Δ47-fPrdm16*$^{-/-}$ FL HSCs, (*n* = 6). (**B**) Representative flow cytometry plots showing gating of LIN$^-$SCA1$^+$cKIT$^-$ (LSK$^-$ cells) in BM of recipients of *Δ47-fPrdm16*$^{-/-}$ (KO) and WT littermate FL cells (*n* = 6). (**C**) Donor LSK$^-$ frequency in recipients of WT and KO FL cells (*n* = 6). (**D**) Ratio of marginal zone (CD21^{hi}CD23^{lo}) to follicular B-cells (CD23^{hi}CD21^{lo}) (MZ/FO) among donor splenic B-cells (CD19$^+$) in recipients of WT and KO FL cells (*n* = 3). (**E**) SCA1 mean fluorescence intensity (MFI) of donor MZ cells (*n* = 3). (**F**) Relative CD150 MFI of FL HSCs (*n* = 54 mice). (**G**) LSK$^-$ frequency (*n* = 73 mice) in FL from WT, *Δ47-fPrdm16*$^{+/-}$ (HET), and KO FL expressed as a percent relative to litter average. (**H**) *Prdm16* mRNA copies/cell in HSC and LSK$^-$ populations from 8 week old wt mice. (*n* = 3-4 mice, in triplicate). (mean ± SEM; n.s:*P* > 0.05; **P* < 0.05; ***P* < 0.01; ****P* < 0.001, One-way ANOVA for multiple comparisons or Student's t-test for single comparisons).

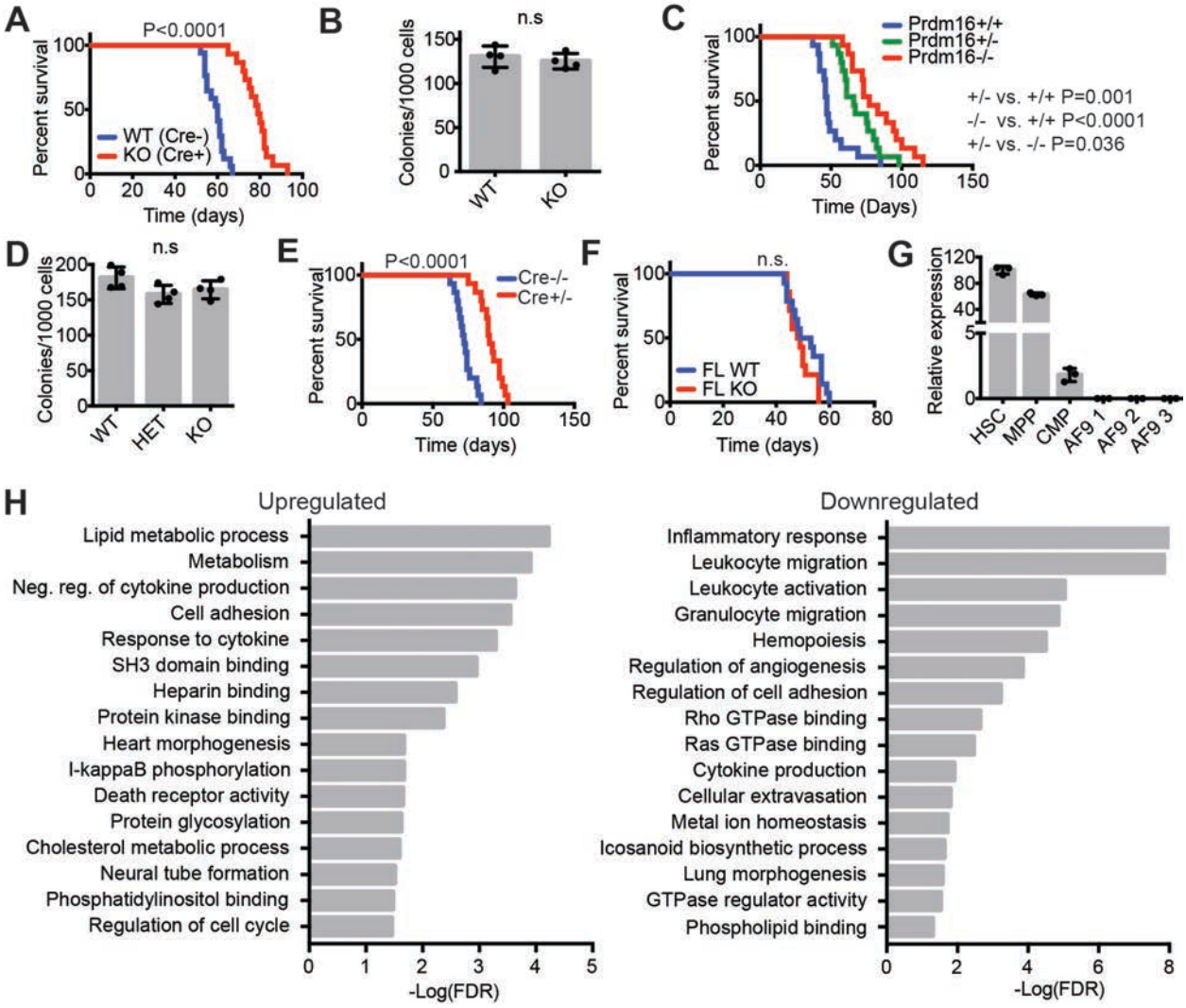

Figure 5: *sPrdm16* expression in HSCs shortens latency of MLL-AF9 leukemia. (**A**) Survival of lethally irradiated mice transplanted with BM HSC-derived MLL-AF9 cells from *Vav-Cre*$^{-/-}$ *Prdm16*$^{fl/fl}$ (WT) and *Vav-Cre*$^{+/-}$ *Prdm16*$^{fl/fl}$ (KO) mice. (**B**) Colony-forming assays of MLL-AF9 cells from (A). (*n* = 4 independent assays in duplicate). (**C**) Survival of lethally irradiated mice transplanted with *Prdm16*$^{+/+}$ (WT), *Prdm16*$^{+/-}$ (HET), or *Prdm16*$^{-/-}$ (KO) FL HSC-derived MLL-AF9 cells. **(D)** Colony-forming assays of MLL-AF9 cells from (C). (*n* = 4 independent assays in duplicate). (**E**) Survival of lethally irradiated mice transplanted with MLL-AF9 cells generated from from BM LIN$^-$SCA1$^-$KIT$^+$ cells from *Vav-Cre*$^{-/-}$ *Prdm16*$^{fl/fl}$ (WT) and *Vav-Cre*$^{+/-}$ *Prdm16*$^{fl/fl}$ (KO) mice. (**F**) Survival of lethally irradiated mice transplanted with FL HSC-derived MLL-AF9 cells from *Δ47-fPrdm16*$^{-/-}$ (KO) or WT littermate mice. (**G**) Expression of *Prdm16* relative to HSC controls in stem and progenitor cells and in MLL-AF9 leukemic cells. (*n* = 3, in triplicate). (**H**) GO pathways significantly up/downregulated in KO relative to WT MLL-AF9 cells from (A). Values expressed as $-\text{Log}_{10}$ of the P-value, determined by PANTHER analysis. (mean ± SEM; n.s:*P* > 0.05; **P* < 0.05; ***P* < 0.01; ****P* < 0.001, One-way ANOVA for multiple comparisons, Gehan-Breslow-Wilcoxon test for comparison of survival curves) (*n* = 13-15, recipients from 3 independently-derived MLL-AF9 lines for each of the survival experiments in (A), (C), (E), and (F)).

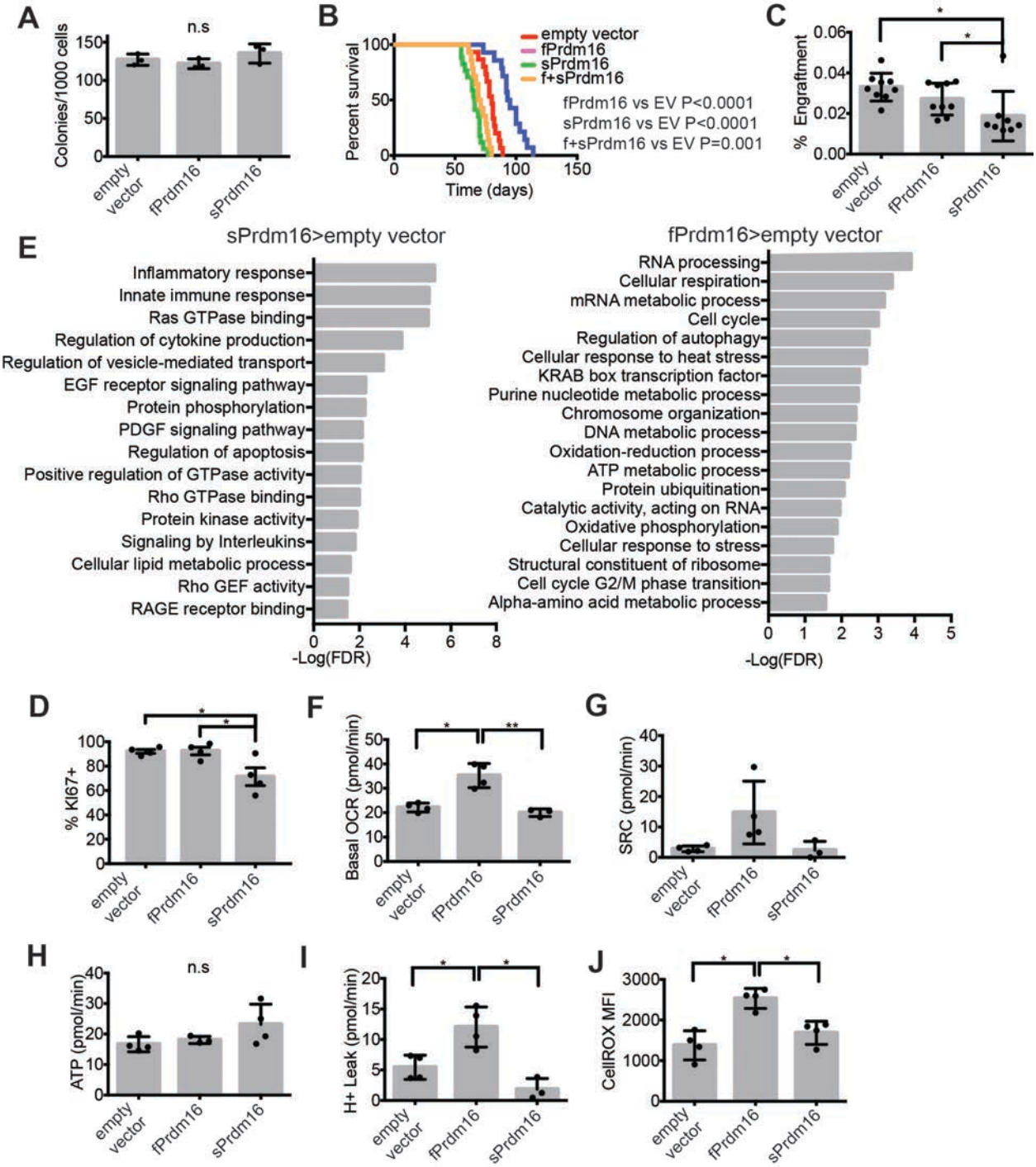

Figure 6: Distinct roles of *Prdm16* isoforms in MLL-AF9 leukemia (**A**) Colony-forming assays of *Prdm16*-deficient *Vav-Cre*$^{+/-}$ *Prdm16*$^{fl/fl}$ (KO) MLL-AF9 cells expressing empty vector, *fPrdm16*, or *sPrdm16*. (*n* = 3 independent assays in duplicate). (**B**) Survival of lethally irradiated mice transplanted with MLL-AF9 cells expressing empty vector, *fPrdm16*, *sPrdm16* or both (*n* = 14-15 recipients from 3 independent experiments). (**C**) Percent of MLL-AF9 cells in BM of recipient mice 24-hours post-transplant. (*n* = 9 recipients from 3 transplants). (**D**) Percent KI67^{+} cells among MLL-AF9 cells of leukemic mice (*n* = 4 recipients). (**E**) GO pathways significantly

upregulated in *sPrdm16* or *fPrdm16*-expressing MLL-AF9 cells isolated from leukemic mice. Values expressed as -Log_{10} of the P-value, determined by PANTHER analysis. (**F**) Basal oxygen consumption rate (OCR), (**G**) Spare Respiratory Capacity (SRC) (*P*[EV/*fPrdm16*] = 0.07, *P*[*fPrdm16/sPrdm16*] = 0.08), (**H**) Respiratory ATP Production, and (**I**) Proton Leak in MLL-AF9 cells from leukemic mice. (*n* = 4 recipients). (**J**) Reactive oxygen species (ROS) measured by MFI of CellROX-Deep Red in MLL-AF9 cells (*n* = 4). (mean ± SEM; n.s:*P* > 0.05; **P* < 0.05; ***P* < 0.01; ****P* < 0.001, One-way ANOVA for multiple comparisons, Gehan-Breslow-Wilcoxon test for comparison of survival curves).

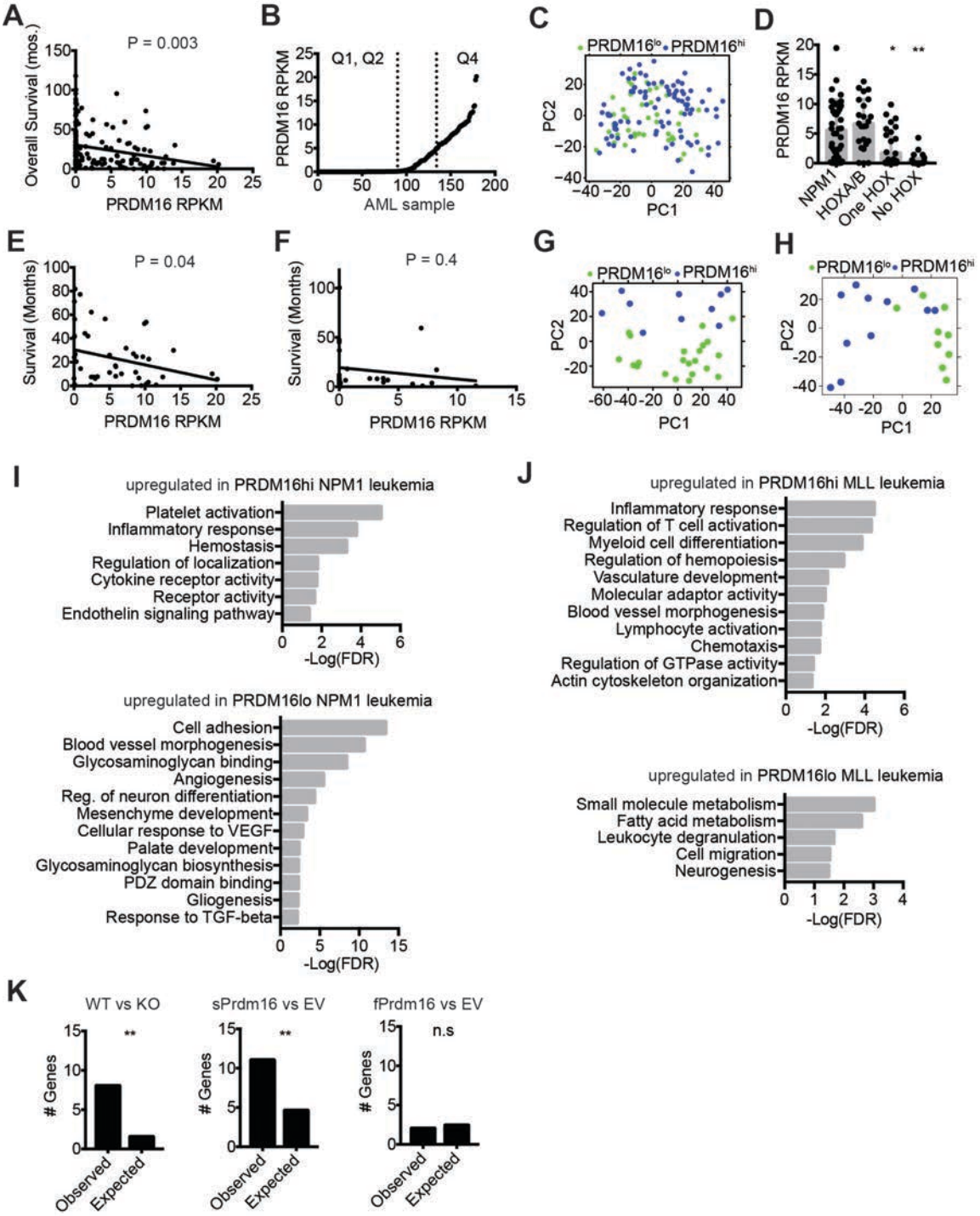

Figure 7: *PRDM16* is associated with an inflammatory signature in a subset of human AML (**A**) Correlation between *PRDM16* RPKM and overall survival in all 179 human AML samples from the Cancer Genome Atlas (CGA) (*n* =179). (**B**) *PRDM16* RPKM for all samples from (A), ranked by RPKM, illustrating Q1/Q2 (*PRDM16*^{lo}) and Q4 (*PRDM16*^{hi}). (**C**) Principal component analysis (PCA) of cohorts described in (B). (**D**) *PRDM16* RPKM compared within 4 mutually exclusive groups from the CGA AML cohort: *NPM1*-mutated, *NPM1wt HOXA9/B4* double-positive (HOXA/B), *HOXA9* or *HOXB4* single-positive (one HOX), and *HOXA9/HOXB4*

double-negative (No HOX) (*n* = 179). (**E**) Correlation between *PRDM16* RPKM and overall survival among *NPM1*-mutated AML samples (*n* = 47) and (**F**) *MLL*-rearranged AML samples in the CGA (*n* = 21). (**G**) PCA of *NPM1*-mutated and (**H**) *MLL*-rearranged AML cases from the CGA, comparing *PRDM16*^{hi} and *PRDM16*^{lo} cohorts. (**I**) Representative list of GO pathways upregulated in *PRDM16*^{hi} or *PRDM16*^{lo} cohorts of *NPM1*-mutated or (**J**) *MLL*-rearranged AML cases in the CGA. Values expressed as $-\text{Log}_{10}$ of the P-value, determined by PANTHER analysis. (**K**) Chi-square analysis of observed vs expected number of dysregulated MDS-related genes in common with genes from our RNAseq analysis in (5H) and (6E). (data represent mean ± SEM; n.s:$P > 0.05$; *$P < 0.05$; **$P < 0.01$; ***$P < 0.001$, Pearson's test for linear correlations, One-way ANOVA for multiple comparisons, Chi-square test for comparing observed vs expected values).